

# In Operando Study of Microsupercapacitors with Gel Electrolytes Using Nano-Beam Synchrotron X-ray Diffraction

Gui Li,<sup>[a]</sup> Nicolas Boulanger,<sup>[a]</sup> Artem Iakunkov,<sup>[a]</sup> Han Xue,<sup>[b]</sup> Jiantong Li,<sup>[b]</sup> Rémi Tucoulou,<sup>[c]</sup> and Alexandre Talyzin<sup>\*[a]</sup>

Synchrotron radiation X-ray diffraction (XRD) with nanoscale beam size was used here for *in situ* and *in operando* study of micro-supercapacitors (MSC) with gel electrolyte and MXene  $Ti_3C_2T_x$  electrodes. The electrode structure was characterized as a function of applied voltage and distance from the gap separating electrodes using microscopic cells with cylindrical shape designed for transmission mode XRD. The devices with gel electrolytes based on  $H_2SO_4$  (with  $H_2O/PVA$  and  $DMSO/PVA$ ) showed stable performance with no changes in MXene structure under voltage swaps between positive and negative values. Experiments with KI-based electrolytes demonstrated changes of MXene structure correlated with decrease of energy

storage parameters under conditions of increased operation voltage starting from 0.8 V. The optimal performance of the MSCs was observed when the MXene structure remained unchanged upon switching the applied voltage polarity. The changes of inter-layer distance of MXene upon swap of applied voltage correlate with decrease of device performance and are undesirable for stable operation of MSC's. We also tested feasibility of X-ray fluorescence (XRF) for characterization of electrolyte ion migration in MSCs using 2D element mapping. Irreversible sorption of iodine by MXene was found using XRF mapping of charged electrodes using standard in-plane MSC device and KI electrolyte.

## Introduction

*In-situ* and *in-operando* studies of energy storage devices attracted a lot of interest in recent years. Synchrotron radiation X-ray diffraction (XRD) and several other methods have been successfully used to study a variety of processes and phenomena directly inside of batteries in the process of charge-discharge.<sup>[1]</sup> However, much less *in-situ* and *in-operando* studies are so far available about supercapacitors.<sup>[2]</sup> One of the main reasons is the rather different mechanism of energy storage in supercapacitors. Electric Double Layer Capacitors (EDLC) store energy by reversible sorption of ions on the surface of the electrode material in the process of charging-discharging.<sup>[3]</sup> Therefore, ideal supercapacitors are not expected to demon-

strate changes in the structure of electrode materials in the process of operation.<sup>[4]</sup> Moreover, the most common electrode materials in industrially produced supercapacitors are porous carbons, which are disordered materials with non-crystalline structure.<sup>[5]</sup> Therefore, X-ray diffraction does not provide much information about these materials. *In-situ* studies of these materials in supercapacitors have been typically performed using other methods, like FTIR or NMR.<sup>[2,6]</sup> X-ray fluorescence (XRF) was also previously used for *in-situ* element mapping of electronic devices,<sup>[7]</sup> but to the best of our knowledge not for studies of supercapacitors.

The amorphous structure of electrodes is not an issue for supercapacitors based on MXene electrodes (most commonly Ti-MXene). MXenes are crystalline layered materials which makes it ideal for model studies of supercapacitors using *in-situ* and *in-operando* XRD.<sup>[8,9]</sup> The changes of MXene structure are very commonly studied by X-ray diffraction revealing a broad range of various phenomena: e.g. swelling in polar solvents, changes in inter-layer distance due to intercalation of various cations, degradation due to oxidation etc.<sup>[10]</sup>

The mechanism of charge storage is not always EDLC and can be different depending on the type of electrolyte. The nearly rectangular shape of cyclic voltammetry (CV) curves observed for MXene in acidic electrolytes (e.g.  $H_2SO_4$ ) have been explained by changes in the Ti oxidation state and protonation of oxygen surface groups.<sup>[11]</sup> Reactions related to titanium oxides ( $TiO$  and  $TiO_2$ ) have been detected *in situ* in the process of cycling by X-ray Absorption Spectroscopy (XAS).<sup>[11b]</sup> XAS is a powerful instrument for evaluation of the oxidation state of Ti, but it does not provide exact information about crystal structures, e.g. not allowing to distinguish between

[a] G. Li, Dr. N. Boulanger, Dr. A. Iakunkov, Prof. A. Talyzin  
Department of Physics  
Umeå University  
SE-901 87, Umeå, Sweden  
E-mail: alexander.talyzin@umu.se

[b] H. Xue, Prof. J. Li  
School of Electrical Engineering and Computer Science  
KTH Royal Institute of Technology  
SE-164 40 Kista, Sweden

[c] Dr. R. Tucoulou  
ESRF The European Synchrotron  
38000, Grenoble, France

 Supporting information for this article is available on the WWW under  
<https://doi.org/10.1002/batt.202400092>

 © 2024 The Authors. Batteries & Supercaps published by Wiley-VCH GmbH.  
This is an open access article under the terms of the Creative Commons Attribution License, which permits use, distribution and reproduction in any medium, provided the original work is properly cited.

crystalline  $\text{TiO}_2$  and surface oxides. Therefore, using XRD for operando study of MXene supercapacitors is complimentary method capable to provide insight into changes of crystal structure and possible appearance of additional phases (e.g.  $\text{TiO}_2$ ).

Individual Ti-MXene sheets are true 2D materials with composition  $\text{Ti}_3\text{C}_2\text{T}_x$  where T refers to surface groups terminating  $\text{Ti}_3\text{C}_2$  layers, such as  $-\text{OH}$ ,  $-\text{F}$ ,  $-\text{Cl}$ .<sup>[12]</sup>  $\text{Ti}_3\text{C}_2\text{T}_x$  is historically the first and most studied MXene in the larger family of transition metal MXenes. It is produced by etching Al away from MAX phase  $\text{Ti}_3\text{AlC}_2$  using suitable acids, most commonly HF.<sup>[12b,13]</sup> Instead of using dangerous HF acid directly, fluoride salts and strong acids are used to form HF *in-situ*, for example by mixing LiF and HCl, which provides much safer and milder routes to produce  $\text{Ti}_3\text{C}_2\text{T}_x$  MXene.<sup>[14]</sup> This type of MXene is also intercalated by Li and often additionally lithiated in LiCl solutions to make distribution of Li cations homogeneous all along the MXene interlayers.

MXene has relatively high specific surface area, good conductivity and favorable mechanical properties for manufacturing flexible devices. Therefore, MXene is widely considered as a promising electrode material for high-performance micro-supercapacitors (MSCs).<sup>[15]</sup> Relatively few studies are currently available about the energy storage mechanism of MXene supercapacitors using *in-situ* techniques.<sup>[16]</sup> For example, *in-situ* X-ray diffraction methods were used to probe the swelling/contraction of  $\text{Ti}_3\text{C}_2$ -MXene interlayers in process of charge-discharge revealing small ( $\sim 0.3 \text{ \AA}$ ) changes in inter-layer distance.<sup>[16f]</sup> Experiments were also performed with ionic liquid electrolytes during the charging and discharging process revealing reversible expansion and shrinking due to a change of applied voltage.<sup>[17]</sup> However, almost all so far reported studies were focused on supercapacitors with aqueous or ionic liquid electrolytes in standard parallel plate supercapacitor devices.<sup>[11b,18]</sup> In-plane microsupercapacitors with gel electrolyte are very common type of devices actively studied in recent years with many electrode materials.<sup>[19]</sup> The in-plane geometry of these devices makes it especially convenient for 2D mapping.

Surprisingly, no structural studies were so far reported for in-plane MSC devices with standard gel electrolytes under conditions of operation. We anticipated that XRD is likely to provide valuable information about the structure of MXene in common gel electrolytes and, possibly, help to reveal structural changes in process of MSC operation under variation of applied voltage or after charge-discharge cycling. Using synchrotron radiation XRD with sub-micrometer sized beam allows also to study structural changes as a function of distance from the material-free separating gap zone on both electrodes. To the best of our knowledge, space resolved XRD experiments with MSC have never been reported previously.

In this work, we designed a special type of MSC cell with MXene electrodes painted directly on the outer surface of standard glass capillaries favorable for transmission mode XRD. The cylindrical MSC covered with  $\text{H}_2\text{O}$  and DMSO based gel electrolytes were characterized using XRD under conditions of charge-discharge with simultaneous electrochemical characterization. The interlayer distance of MXene electrodes was

monitored *in-situ* after the voltage swaps in fully charged state and *in-operando* during charging/discharging. Our results demonstrate a strong difference between nearly complete absence of changes of MXene structure in "good" ( $\text{H}_2\text{SO}_4$ -based) and strong changes of structure in "poor" (Kl-based) gel electrolytes. In addition, we tested feasibility of synchrotron radiation X-ray fluorescence for mapping of electrolyte ion distribution in gel MSC after charging and discharging of electrodes.

## Experimental Section

### MXene Synthesis and Characterization

3 grams of lithium fluoride (Merck) were mixed with 60 mL of 9 M hydrochloric acid (Merck) and the solution was kept stirring for 30 min. Then 3 grams of the MAX precursor  $\text{Ti}_3\text{AlC}_2$  (Merck) were then gradually added to the dispersion. The solution was kept under stirring at 45 °C for 45 h. Afterwards, 40 mL of distilled water was then added, and the solution was washed using 6 M hydrochloric acid which was removed by centrifugation at 20 000 rpm for 20 min repeated 6 times. The sediments were then preserved and mixed within a 1 M lithium chloride (Merck) solution and kept under argon for 24 h. The solution was then centrifuged at 20 000 rpm for 20 min to recover the sediments. Subsequent washing was then done using centrifugation at 20 000 rpm for 20 min repeated 6 times using distilled water. Finally, water was added to the sediment and mild centrifugation was done 3 times at 1000 rpm for 10 min, 800 rpm for 10 min and 500 rpm for 5 min, with the supernatant being collected and more added more water after each centrifugation step. The supernatant was vacuum filtered and re-dispersed in water to prepare a solution later used to make the electrodes. A slightly different procedure was used to prepare MXene for the printed microsupercapacitors (see SI file).

The MXene synthesis was performed 1 week prior to the experiments at ESRF in order to avoid possible ageing issues. It is known that MXene degrades over time with the formation of Ti oxides,<sup>[20]</sup> especially if stored in water or under humid air,<sup>[21]</sup> but also in variety of solvents.<sup>[20,22]</sup> A decrease in conductivity was consistently observed with longer exposure times.<sup>[23]</sup> Experiments were performed with MXene after 1 week of storing it in water (under argon) with XRD revealing only rather small trace of Ti oxides (Figure 1S, 2S, 3S in SI file). A detailed study of MXene degradation in water is out of scope of this study.

The freshly deposited MXene from the same batch was characterized by XRD in a wet state (with some water remaining) prior to experiments (Figure S1 and S2 in SI file). SEM images recorded from dried MXene powder showed some aggregates and individual  $\mu\text{m}$ -sized flakes (Figure S4). Characterization of MXene prepared using the same procedure was also performed in our earlier studies using XPS, TGA and FTIR, SEM confirming successful synthesis and the good quality of MXene in agreement with literature data.

### Preparation of Microsupercapacitors and Electrolyte

MSC were prepared using two different designs. The first design was used for XRD experiments in order to provide favourable for transmission mode geometry of MXene layers. The cylindrical microsupercapacitors (CMSC) were prepared by painting both electrodes on the outside of glass capillaries using wet MXene paste (Figure 1a). The gel electrolyte was directly deposited over the pair of electrodes and the material-free gap. The glass

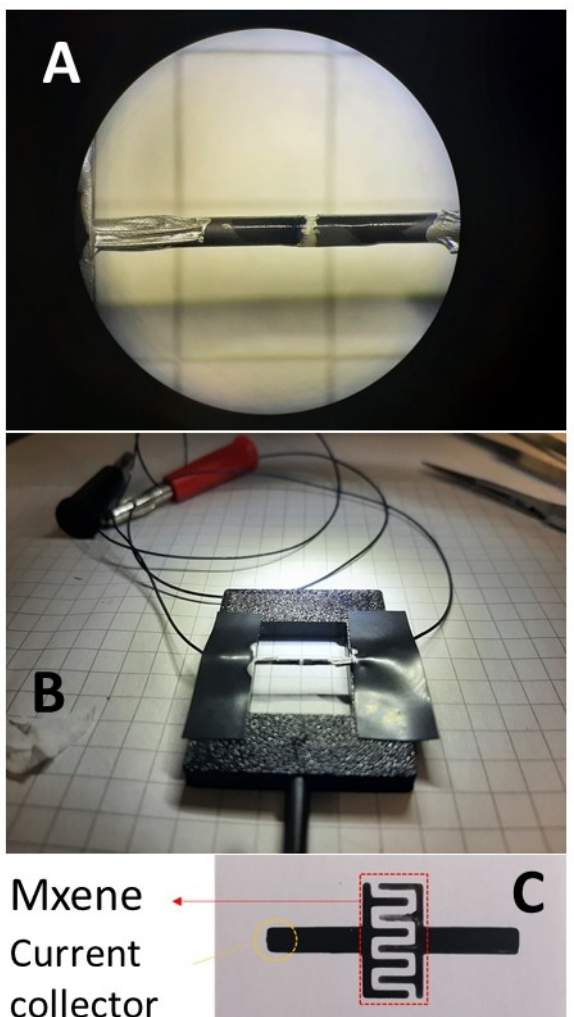


**Figure 1.** a) Optical microscopy images of cylindrical microsupercapacitor (CMSC) cell painted on glass capillary and connecting wires attached with silver paste, b) cell assemblage for *in situ* XRD experiments (the size of squares on the paper is 5 mm) and c) example of standard printed in-plane microsupercapacitor.

capillaries were attached to the sample holder frame (Figure 1b) with electrodes connected to a potentiostat (Autolab PGSTAT204). The potentiostat was placed inside the experimental hutch and controlled remotely. Cyclic voltammetry was recorded to verify that the capacitors were functional. Constant potential was applied during the recording of X-ray diffraction patterns.

The electrodes were coated on a 1 mm diameter glass capillary shortly before XRD experiments, dried in air and immediately covered with gel electrolyte. All CMSC devices were prepared no more than 1–2 hours prior to the start of XRD tests.

The second design was used for XRF experiments. The electrodes were printed on Kapton foil thus producing standard in-plane devices (Figure 1c). A Felix bioprinter was used for direct ink printing. The pattern was pre-designed by G-Code and printed under the control of an open-source software (Repetier-Host). To ensure smooth printing, Drifton precision stainless dispensing tips with an inner diameter of 0.4 mm were used. The extrusion amount and moving speed were controlled at constant values of 0.01 mm and 100 mm/min, respectively.

The electrodes were printed several days prior to experiments and covered by fresh electrolyte shortly before the tests at ESRF or directly at ESRF for cylindrical devices painted on glass capillaries. Gel electrolytes were prepared by mixing poly (vinyl alcohol) (Mw 89 000–90 000, Merck) with either 1 M sulfuric acid (Merck) or 0.21 M potassium iodide (Merck). The weight ratio of 1 g of poly (vinyl alcohol) for 10 mL of solution was used. The dispersions were heated at 90 °C for DMSO electrolyte or at 120 °C for KI electrolyte with water as solvent and stirred until it became clear.

### XRF and XRD Experiments

XRF and XRD experiments were carried out at the hard X-ray nanoprobe beamline ID16B of the European Synchrotron (ESRF, France). The X-ray beam was monochromatized with a Si(111) fixed-exit double-crystal monochromator and focused using Kirkpatrick-Baez mirrors. The incident energy of the photon beam was set to 33.5 keV and the focused beam 70×70 nm<sup>2</sup> with an incoming flux of 6e09 ph/s. The experimental setup with the mounted sample is shown in the Figure 1B.

XRD images were recorded in transmission mode using radiation wavelength  $\lambda = 0.37 \text{ \AA}$ . Cylindrical microsupercapacitors painted on standard Hilgenberg glass capillaries with diameter 1 mm were mounted horizontally and perpendicular to the incident beam (Figure S6) focusing most often on the bottom part. For experiments with voltage swaps, XRD images were recorded at the working electrode from the spot located about 0.1–0.2 mm from the gap separating electrodes. Linear scans were performed using the horizontal movement of the sample with steps 0.1 mm over the region of 2 mm which includes both electrodes and the gap zone.

The XRF signal was recorded using two multi-element Silicon Drift Detector (SDD) arrays. XRD was recorded using a FReLoN CCD camera equipped with a fibre optics taper with an effective pixel size of 50×50 μm.

## Results and Discussion

### MSC Cell Setup for In-Operando XRD Characterization

Experiments with XRD and XRF were performed using two types of MSC cells. Initial tests were performed using standard in-plane supercapacitors printed on thin glass support or on Kapton foil (Figure 1C). This design is standard for MSC devices with hundreds of publications available up to the moment, see e.g.<sup>[24]</sup> This setup allows to record XRF data but appeared to be not suitable for XRD characterization in the transmission mode. Experiments were performed at ID16b beamline of ESRF which provides sub-micrometer size X-ray beams (70×70 nm in these experiments) in transmission mode and limited possibilities to rotate the sample. The (001)-reflection of MXene could not be recorded in transmission mode with the beam approximately normal to the MSC plane due to unfavourable preferential orientation of MXene flakes parallel to the substrate (see Figure S6 for details).

Therefore, we designed a new type of cell with electrodes directly painted on the outer surface of standard glass capillaries typically used for XRD experiments with a diameter of 1 mm (Figure 1a). A gap zone with ~0.3–0.5 mm width was scratched away (as accurately as possible) by thin needle to

separate electrodes. Gel electrolyte was added over the surface of CMSC. The cell was mounted in horizontal geometry allowing scans along the length of the capillary using relatively a small 70 nm size X-ray beam.

It should be noted that the design of cylindrical cells imposes limitations to the amount of added electrolyte (due to microscopic size and geometry), but remains to be essentially the same as in in-plane MSC. Electrolyte is added in MSC as a droplet over the surface of electrode, in most cases without sealing or other preventive measures against solvent evaporation.<sup>[19a,24b]</sup> Therefore, slow ageing of gel electrolyte over several days or weeks is an inherent part of the MSC standard design. Microscopic size of our cells allows to study essentially the same ageing processes over few hours instead of days due to smaller amount of electrolyte.

Gel electrolytes based on PVA with water solutions of H<sub>2</sub>SO<sub>4</sub> and KI were tested. The H<sub>2</sub>SO<sub>4</sub> electrolyte was selected because it is the most common choice for MXene supercapacitors. Potassium iodide was selected as electrolyte since iodine is one of chemical elements which can be easily imaged using XRF. We note that the distribution of sulphur in H<sub>2</sub>SO<sub>4</sub> electrolyte could not be imaged using XRF due to the method limitations of ID16b. Since MXene is known to exhibit especially good stability in DMSO solvent, we also tested gel electrolytes based on DMSO solutions of KI and H<sub>2</sub>SO<sub>4</sub>.

## In Situ Characterization of CMSC with H<sub>2</sub>SO<sub>4</sub>+H<sub>2</sub>O/PVA Gel Electrolyte

The CMSC device with gel H<sub>2</sub>SO<sub>4</sub>+H<sub>2</sub>O/PVA electrolyte was tested first before the start of XRD experiments by recording several CV cycles. Considering its rather small size, the device demonstrated good quality CV curves with a shape close to rectangular (Figure 2a). It is known that the mechanism of charge storage for MXene in 1 M H<sub>2</sub>SO<sub>4</sub> is pseudocapacitive, which is reflected in the shape of the CV curve shown in Figure 2a.

The change in titanium oxidation state caused by applied potential is related to protonation of oxygen functional groups according to earlier studies.<sup>[11,25]</sup>

The XRD patterns were recorded then from the electrode spot located close to the gap in the charged state under applied voltage +0.6 V (with zero volt on counter electrode). To ensure saturated charging, current curves vs time were recorded before taking XRD images. XRD images were recorded after reaching a plateau on current vs time curve. Typically, the current dropped to zero after about 100 sec (example in Figure 2b). In the next step the voltage was changed to -0.6 V repeating the procedure with an XRD image recorded after full charging of the electrode. Three complete cycles were recorded using voltage swap +0.6/-0.6 V, voltage swaps +0.8/-0.8 V, voltage swaps +0.9/-0.9 V and finally voltage swaps +1.0/-1.0 V.

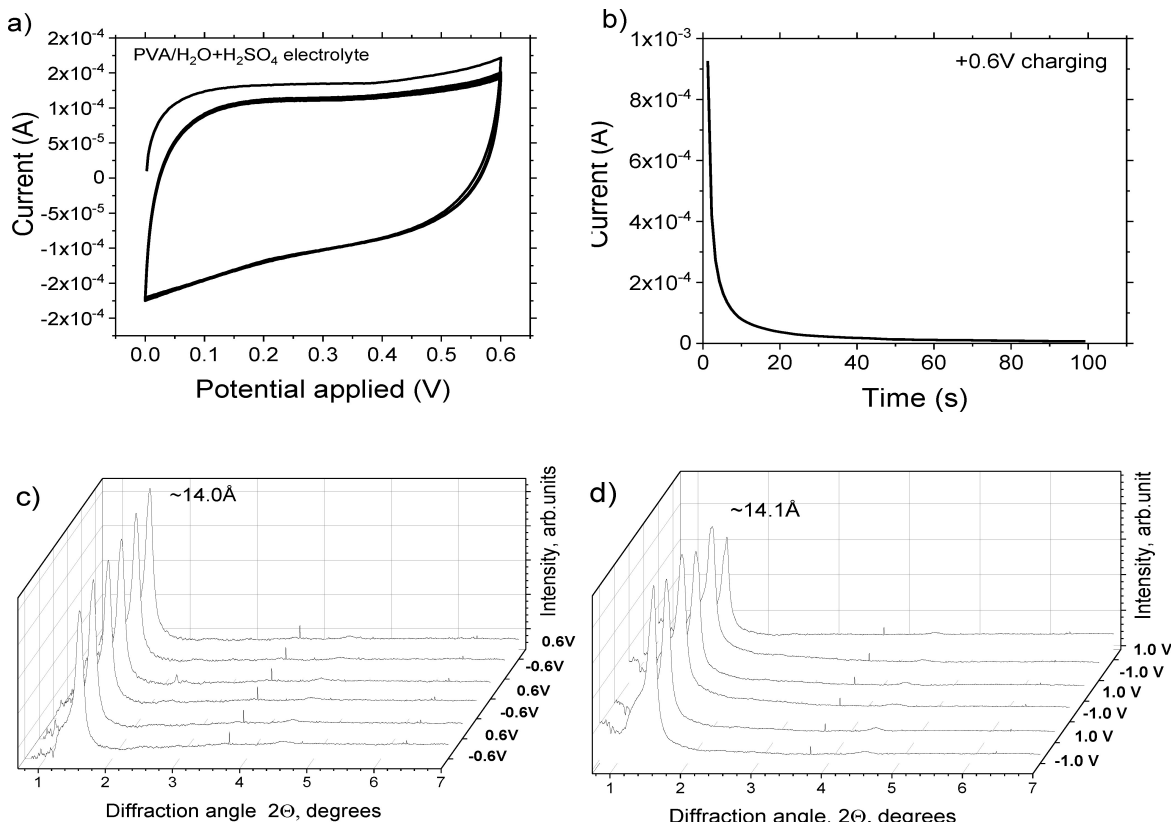


**Figure 2.** CV curve recorded with scan rate 50 mV/s prior to start of XRD characterization (H<sub>2</sub>SO<sub>4</sub>+H<sub>2</sub>O/PVA gel electrolyte) to check the device performance (a), example of charging curve recorded at +0.6 V until saturation is achieved (b), XRD patterns (background subtracted) recorded from working electrode (with zero volt at counter electrode) at fully charged state with applied voltage swaps between +0.6 and -0.6 V (c) and +1.0 V and -1.0 V (d). Similar data for voltage swaps +0.8 V/-0.8 V and +0.9/-0.9 V are provided in SI file. Radiation wavelength  $\lambda=0.370\text{ \AA}$ .

–1.0 V (Figure 2b). The XRD data recorded from positively and negatively charged MXene electrode showed no changes in the inter-layer distance. The  $d(001)$  value in the range 14.0–14.1 Å was recorded in all scans performed with positive and negative applied voltage in the whole tested range (0.6–1.0 V) (Figure 2c and d).

On the next step, the same device was studied *in-operando* with XRD images recorded continuously during the process of recording CV curves. Similarly to experiments with XRD recorded at static fully charged conditions, no changes in position of (001) reflections were recorded in two *in operando* experiments performed with 0 to +1 V and 0 to –1 V cycling.

The (001)-reflection position remained the same during the cycles within 14.4–14.8 Å which is somewhat higher than the value recorded in static experiments. The shape of CV curves recorded during the cycles was also somewhat different (see insets in the Figure 3) and less rectangular, as expected for voltages over 0.6 V according to literature data. Similar shape of CV curves was observed for MXene in  $\text{H}_2\text{SO}_4$  electrolyte in the same voltage window e.g. in ref.<sup>[26]</sup>

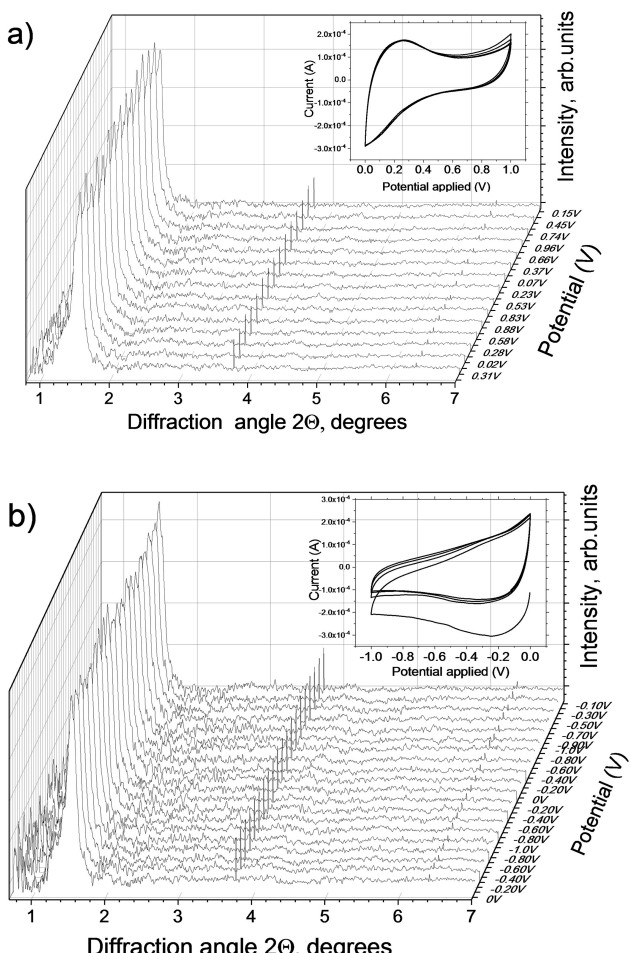


**Figure 3.** XRD patterns recorded in operando under conditions of CV cycling ( $\text{H}_2\text{SO}_4 + \text{H}_2\text{O}$  gel electrolyte). a) for positive and b) negative potentials applied to the working electrode (keeping second electrode at zero potential). Insets show CV curves (scan rate 50 mV/s). Only each second of recorded patterns are shown (background subtracted). XRD pattern recorded in material-free gap was used to subtract background.  $\lambda = 0.370 \text{ \AA}$ .

The cylindrical shape of the MSC device and the horizontal orientation of capillary perpendicular to the incident X-ray beam allowed also to record linear scans along the length of the capillary starting from the active electrode, over the material-free gap and finally over the counter electrode (Figure 4).

The value of  $d(001)$  registered along the whole length of the 2 mm scans was about 15 Å in both electrodes and in both scans performed with applied voltage +1 V and –1 V. The scatter in  $d(001)$  values is explained by the presence of diffraction spots (rather than perfect diffraction rings) in the recorded images reflecting the incompletely homogeneous structure of the electrode deposited by simple drying of water based MXene paste without any binder and preferential orientation of 2D sheets parallel to the substrate.

Summarizing results obtained using XRD in the *in-situ* and *in-operando* experiments with CMSC with  $\text{H}_2\text{O}-\text{H}_2\text{SO}_4$  electrolyte, the structure of MXene is found to be surprisingly stable even at highest tested applied voltage of 1 V/–1 V. The electrode material is found to be stable in the fully charged state with different polarity and under conditions of charge-discharge. Moreover, the structure remains to be the same at least 0.5 mm away from material-free gap zone revealing no spatial variation. The only observed change of structure was a slow increase of  $d(001)$  during the process of experiments. The initial  $d(001) = 14.0\text{--}14.1 \text{ \AA}$  recorded under gel electrolyte had increased in the last experiments (Figure 4) up to ~15 Å. The increase of applied voltage from 0.6 V to 1 V also resulted in some change in CV curves shape and lower charging capacity of electrodes.

The values of  $d(001)$  recorded under the gel electrolyte are larger than the value recorded in air in a solvent-free state (11.8 Å) from the MXene powder sample. It is also significantly smaller than the value recorded from freshly prepared MXene in excess of water in a pristine paste (~20.5 Å). Therefore, swelling of MXene in water-based  $\text{H}_2\text{SO}_4/\text{PVA}$  gel electrolyte is much smaller than in pure water but the increase of inter-layer distance is sufficient for penetration of both  $\text{H}^+$  and  $\text{SO}_4^{2-}$  ions. The size of the sulphate anion is ~2.4 Å.<sup>[27]</sup> The size of inter-layers available for penetration of ions can be then calculated as the difference between the “dry” state (~12 Å) and electrolyte-swollen state (~15 Å) providing a value of ~3 Å. This value correlates approximately with the thickness of one water layer confined between MXene flakes.<sup>[28]</sup> Similar thickness of a water layer have been also reported for other hydrophilic layered materials with the ability to swell in water, e.g. clays<sup>[29]</sup> and graphite oxides.<sup>[30]</sup>

It is interesting to compare our *in situ* XRD data to earlier studies of changes in MXene structure due to anodic oxidation.<sup>[31]</sup> Reversible “pseudocapacitive” oxidation of Ti was reported for MXene in  $\text{H}_2\text{SO}_4$  electrolyte at low voltage, without formation of  $\text{TiO}_2$  (according to both XRD and Raman spectroscopy data).<sup>[11b]</sup> Irreversible oxidation of Ti at applied potential of 0.8 V is well documented in literature but the exact mechanism of Ti oxidation is still somewhat unclear. Formation of crystalline  $\text{TiO}_2$  was not confirmed in our *in situ* experiments, also it was not found in experiments with ex-situ character-

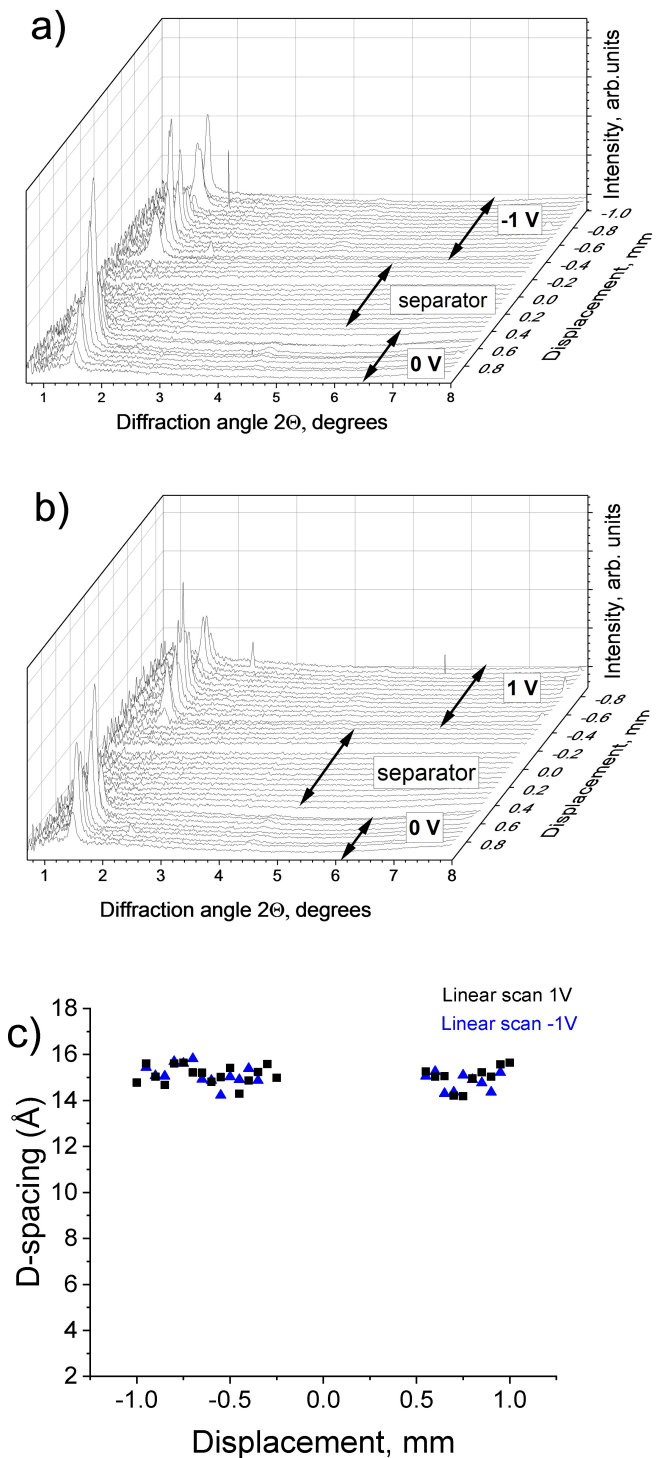


**Figure 4.** XRD patterns ( $\lambda = 0.370 \text{ \AA}$ ) recorded in the linear scan along the length of CMSC over the material-free gap and MXene electrodes ( $\text{H}_2\text{SO}_4 + \text{H}_2\text{O}$  gel electrolyte) under applied voltages  $-1 \text{ V}$  (a) and  $+1 \text{ V}$  (b) with counter electrode at  $0 \text{ V}$ . (c)-values of d-spacings along the studied length for scans shown in (a) and (b). One of the XRD patterns recorded in the middle of material-free gap was used to subtract background.

ization of MXene electrodes after anodic oxidation with applied potential up to  $0.9 \text{ V}$  in ref.<sup>[31]</sup>

XRD would not reveal formation of amorphous Ti oxides but in this case degradation of MXene structure is unavoidable. In contrast, both our XRD data and ex-situ data presented in ref.<sup>[31]</sup> do not show clear signs of MXene structure collapse even after cycling at  $0.9\text{--}1.0 \text{ V}$ . Moreover, the same value of inter-layer distance of  $14\text{--}15 \text{ \AA}$  is found in our experiments with XRD recorded directly under gel electrolyte and in ex-situ experiments presented in ref.<sup>[31]</sup> The increase of inter-layer distance from  $\sim 12 \text{ \AA}$  (in pristine solvent free state) up to  $14 \text{ \AA}$  already after cycling at  $0.1 \text{ V}$  was assigned in Ref.<sup>[31]</sup> to effects of Ti oxidation, but it was not verified with reference sample simply immersed in  $\text{H}_2\text{SO}_4$  electrolyte and dried. Therefore, irreversible sorption of sulphuric acid was not ruled out as a reason for the  $2 \text{ \AA}$  increase of inter-layer distance in MXene.

As a simple test to verify this alternative explanation of MXene lattice expansion we performed additional ex-situ experiment by recording XRD patterns from pristine MXene, MXene immersed in  $1 \text{ M H}_2\text{SO}_4$  solution and the same sample after air drying. Pristine MXene showed d-spacing corresponding to interlayer distance at  $12.08 \text{ \AA}$ . Swelling of MXene in  $1 \text{ M H}_2\text{SO}_4$  resulted in expansion of inter-layer distance up to  $14.45 \text{ \AA}$ , very similar to our *in situ* experiments with supercapacitors. The same sample after several hours of air drying showed two reflections, first corresponding to pristine MXene  $d(002) = 12.2 \text{ \AA}$  and second with  $d(002) = 15.2 \text{ \AA}$  which likely corresponds to the MXene intercalated with sulphuric acid. This experiment provides additional evidence for swelling and intercalation with sulphate ions as a reason for earlier reported MXene lattice expansion from  $12 \text{ \AA}$  to  $15 \text{ \AA}$ .

Therefore, we believe that surface oxidation of Ti in  $\text{Ti}_3\text{C}_2$  layers is unlikely to be a reason for the expansion of the MXene lattice from  $12 \text{ \AA}$  up to  $14 \text{ \AA}$ . The most probable result of irreversible oxidation of Ti in MXene would be the formation of a separate amorphous phase not detectable by XRD. The  $14 \text{ \AA}$  inter-layer distance is related to swelling of MXene in water-based  $\text{H}_2\text{SO}_4$  gel electrolyte. As demonstrated in the next section swelling of MXene in DMSO based  $\text{H}_2\text{SO}_4$  electrolyte results in significantly stronger swelling with inter-layers distance of about  $18 \text{ \AA}$  in agreement with earlier literature data on swelling of MXene in pure DMSO.<sup>[10b,f,32]</sup>

The electrochemical data recorded in our study *in-situ* and *in-operando* provide evidence for migration of ions in and out of the MXene structure without additional effects related to the change of inter-layer distance. In principle, the change of inter-layer distance due to migration of ions to and from the surface of individual MXene flakes is an undesirable effect as it would strongly affect the kinetics of ions intercalation and charge-discharge parameters of the MSC cell. It should be noted that  $\text{H}_2\text{SO}_4$  is considered as one of the best electrolytes for operation of MXene supercapacitors. Our experiments confirm that absence of voltage-induced swelling and changes of inter-layer distance related to insertion and de-insertion of electrolyte ions are parameters which can be considered as signs of a "good" electrolyte for MXene MSC. However, that is not the case for an electrolyte based on KI as described below.

### In Situ Characterization of CMSC with $\text{H}_2\text{SO}_4$ -DMSO Electrolyte

DMSO was selected in these experiments due to the strong swelling of the MXene in this solvent.<sup>[10b,33]</sup> It was anticipated that stronger changes in MXene interlayer distance will be observed if DMSO is used as a solvent for  $\text{H}_2\text{SO}_4$  instead of water.  $\text{H}_2\text{SO}_4$  dissolves in DMSO thus allowing to prepare gel electrolytes with PVA. Indeed, the changes in the structure of MXene electrodes appeared to be significantly different for DMSO and  $\text{H}_2\text{O}$ -based electrolytes. Experiments with DMSO- $\text{H}_2\text{SO}_4$  electrolyte were performed first at static conditions in a fully charged state with a swap of applied voltage from positive to negative values at 0.6 V, 0.7 V, 0.8 V, 1.0 V and 1.1 V in order to study the MXene structure at voltage values which typically result in the degradation of MSC energy storage parameters. Figure 5 shows a CV curve recorded from freshly prepared CMSC prior to XRD tests.

The device with DMSO-based gel electrolyte showed reasonably good performance with CV curve shape and energy storage similar to the device with water based  $\text{H}_2\text{SO}_4$  electrolytes (Figure 2). The CV curves recorded after voltage swaps at a

higher voltage of 0.9 V/–0.9 V showed nearly complete degradation of the device. The degradation of the device can be correlated with a strong change in XRD data. The structure of MXene electrode in DMSO- $\text{H}_2\text{SO}_4$  gel electrolyte remained unchanged after voltage swaps at 0.6/–0.6 V and 0.7/–0.7 V (Figure 5c) with inter-layer distance of ~18.2 Å. This value of inter-layer distance is in good agreement with our data reported earlier for swelling of similarly prepared MXene in pure DMSO (~18 Å at ambient temperature, see Figure S2 in SI file and ref.).<sup>[10b]</sup> Further increase of applied voltage to 0.9/–0.9 V results in dramatic changes of MXene structure. New reflection with  $d \sim 22$  Å corresponds to expanded (001) lattice.

It is interesting that the new reflection which appears in the MXene electrode under full charging with 0.9/–0.9 V applied voltage has the same  $d$ -spacing (~22 Å) as the (001) reflection recently found in our experiments with temperature dependent swelling of MXene in DMSO above ~360 K. The difference in  $d$ -spacing values of ~4 Å can be then assigned to intercalation of additional DMSO layer. It is rather unlikely that electrodes were heated above 360 K in our SMSC device. Therefore, our results demonstrate that the 2-layered phase of MXene-DMSO can be produced not only by an increase of temperature but also by

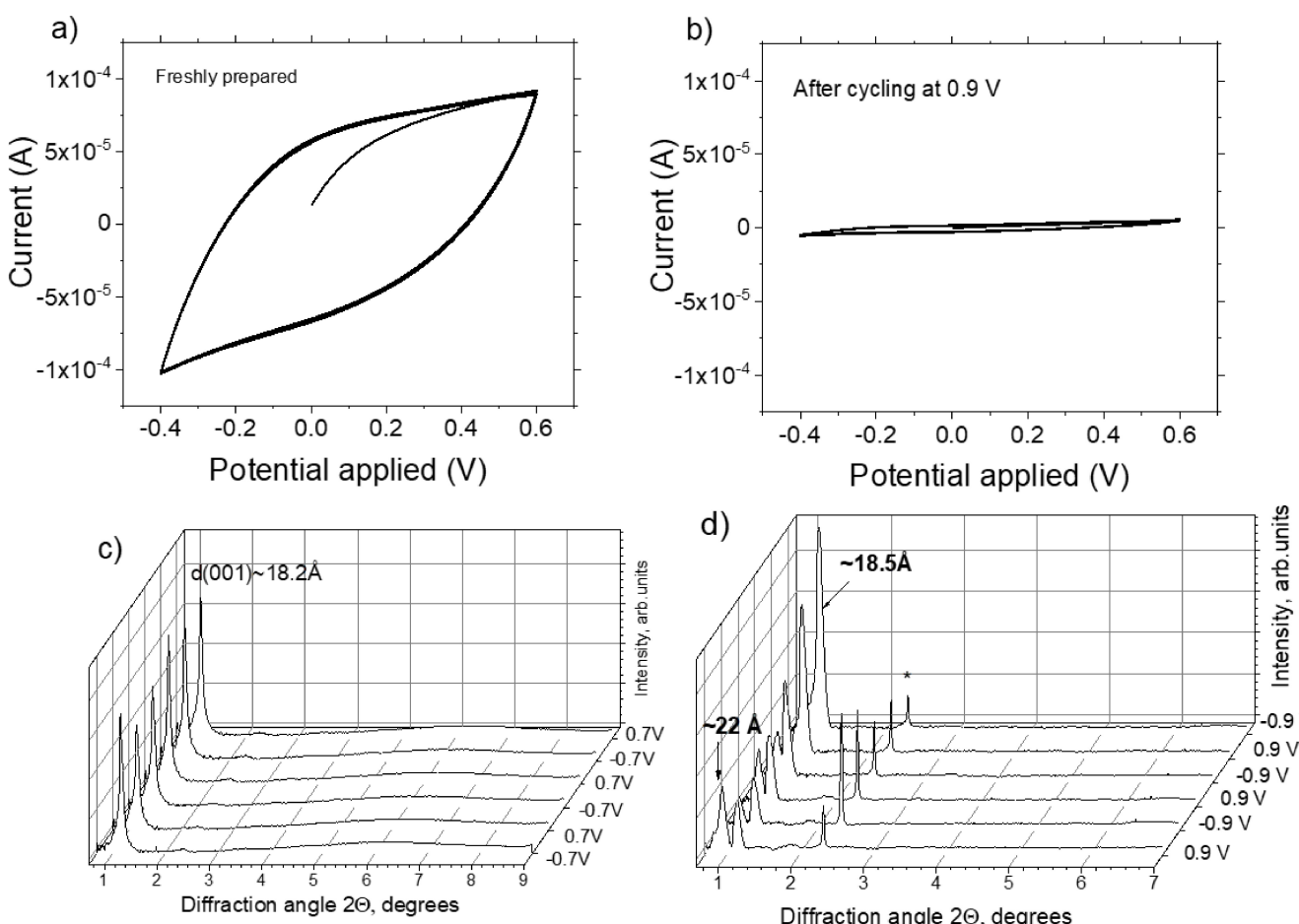


**Figure 5.** CV curves recorded from freshly prepared CMSC ( $\text{H}_2\text{SO}_4$ +DMSO gel electrolyte) with scan rate 50 mV/s (a) and from the same device after *in situ* XRD experiments with swap of applied voltages at 0.6 V, 0.7 V, 0.8 V and 0.9 V (b); XRD data recorded from working electrode under static conditions of saturated charging at voltages swap 0.7/–0.7 V (c) and 0.9 V/–0.9 V (d). The peak shown by star is due to single spot. The data recorded with applied voltages 1.0 V/–1.0 V and 1.1 V/–1.1 V are shown in SI (Figure S4).  $\lambda = 0.370\text{\AA}$ .

voltage swap at ambient temperature. Alternatively, it might be related also to chemical modification of MXene surface or redistribution of Li intercalated in MXene inter-layers. The exact reasons controlling inter-layer distance in MXene electrodes in these experiments cannot be resolved using our XRD data. It can be concluded that the structure of the working electrode is inhomogeneous consisting of two phases with different inter-layer distance, which is reflected in the degradation of electrochemical performance (Figure 5d).

Further increase of voltage in the swaps to 1.0 V/–1.0 V resulted only in some broadening and overall decrease of intensity for all XRD reflections, while after 1.1/–1.1 V swaps the intensity of all peaks dropped rather significantly (see SI file) thus providing evidence for complete degradation and amorphization of the electrode material. Our attempt to perform a linear scan over the working and counter electrode after completion of experiments with voltage swaps was not successful due to the rather low intensity of XRD reflections.

Our experiments demonstrate that DMSO is a less suitable solvent for  $\text{H}_2\text{SO}_4$  gel electrolyte in MXene MSC as compared to water. Electrochemical performance and structural stability of MXene under conditions of applied voltage in MSC are a lot better if  $\text{H}_2\text{SO}_4$  is dissolved in water as compared to DMSO- $\text{H}_2\text{SO}_4$ .

#### XRF and XRD Characterization of CMSC with $\text{KI} + \text{H}_2\text{O}$ Electrolyte

#### Feasibility of XRF for Element Mapping In-Situ in In-Plane MSC Devices

Iodine is a chemical element which can be easily mapped using XRF.<sup>[33]</sup> Therefore, our initial experiments with KI electrolyte

were aimed at demonstrating the possibility of using XRF for 2D element mapping of MSC under conditions of applied voltage. Standard in-plane MSC devices with MXene electrodes (see Figure 1C) were printed on Kapton foil for these experiments. However, test experiments demonstrated that detailed study of iodine migration in the MXene electrodes and gel electrolyte is not trivial due to the difficulty of controlling the thickness of the electrolyte layer. Typically gel electrolyte is added as a droplet over the flat surface of in-plane MSC. When the electrolyte gel is added with large excess as in standard devices, the change in iodine concentration was not detected. Moreover, no difference in concentration of iodine was detected over the electrode and gap regions. When the electrolyte layer was added as a very thin layer, iodine was detected only over the electrodes but not in the gap zone. Moreover, no change in iodine concentration was detected in this case under conditions of applied voltage (see SI file). Obviously, the amount of ions in the very thin layer of gel electrolyte was so small that all iodine got absorbed by MXene after the initial test of device performance. Finally, we were able to prepare devices with an electrolyte layer sufficiently thick for operation of MSC, to detect the change in concentration due to applied voltage and to see clear concentration contrast between the region of material-free gap and electrodes (Figure 6).

The 2D mapping clearly shows bright regions with high Ti concentration at MXene electrodes and a black material-free gap ( $\sim 1$  mm). The iodine mapping still shows the differences in concentration over the gap region but is much less sharp and possibly affected by the shape of the gel droplet. The most important result of the XRF experiment is the demonstration of strong and irreversible sorption of iodine by MXene electrodes. Note that both experiments shown in Figure 6 and Figure S5 (SI file) show a deep valley in the concentration of iodine

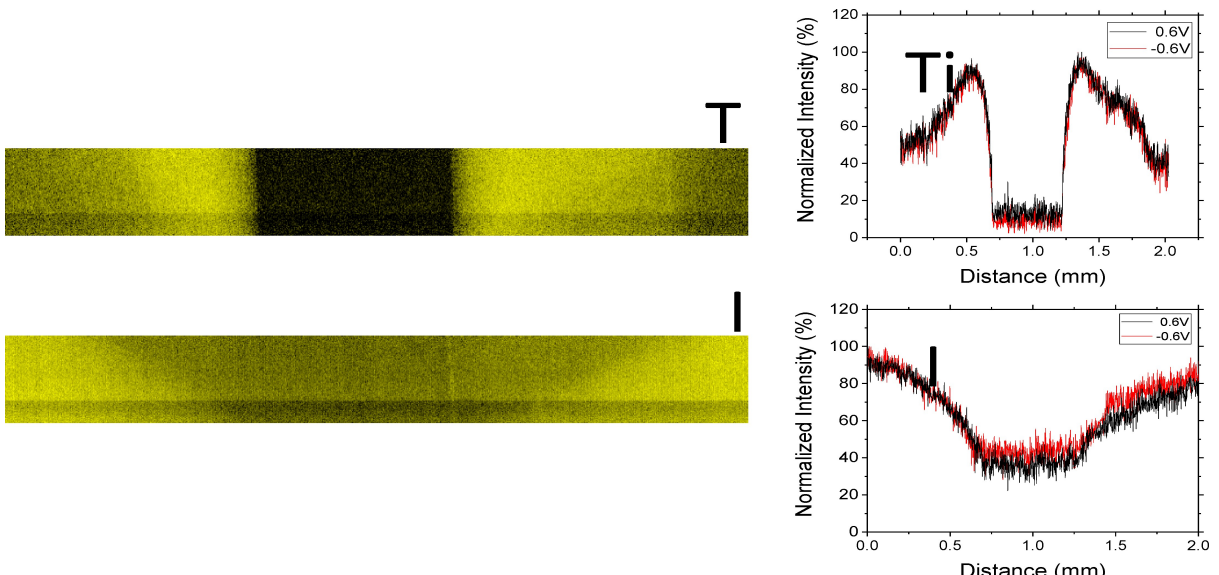


**Figure 6.** 2D images recorded using XRF showing Ti and Iodine concentration in the area of electrode separating gap for printed in-plane MSC with MXene electrodes ( $\text{KI} + \text{H}_2\text{O}$  gel electrolyte). The length of shown region is 2 mm. The change of integrated profiles under conditions of changed polarity of applied voltage is shown in two diagrams, for Ti and I. Some change in the concentration of iodine can be detected on the right side.

corresponding to the material-free region of the MSC device independently of the charging state of the electrode. In the ideal case of negligible sorption, complete migration of iodine to the positively charged electrode would be observed. Since the thickness of the gel electrolyte layer is approximately the same over the 2 mm observation zone, an excess of iodine in electrodes is a clear sign of irreversible (by change of voltage polarity) sorption of iodine anions.

The data shown in Figure 6 demonstrate that the 2D element mapping of MSC using XRF is feasible but requires precise control over the thickness of the gel electrolyte layer in order to provide more information about charge-discharge processes over the electrodes. Therefore, we focused on XRD experiments with MXene CMSC and KI + H<sub>2</sub>O gel electrolyte.

#### In Situ XRD Characterization

XRD patterns recorded from the MXene electrode covered with KI + H<sub>2</sub>O gel electrolyte (after initial testing with three CV loops) (Figure 7b)) showed two (001)-reflections with d-spacings ~14.6 Å and ~18.1 Å. The smaller d-spacing is likely corresponding to inter-layers filled only with water (similar to experiments with H<sub>2</sub>SO<sub>4</sub> electrolyte). The d-spacing of 18.1 Å is significantly larger and should be assigned to intercalated inter-layers of MXene. The swap of applied voltage polarity has not resulted in a change of peak positions or a change in relative intensity. Considering the irreversible sorption of iodine detected by XRF, we suggest that the lattice expansion to 18.1 Å is related to

intercalation of iodine but XRD data does not allow unambiguous interpretation of the structure change. However, we note that 3.5 Å increase of MXene c-lattice is similar to the effective size of iodine (~4 Å).<sup>[34]</sup>

Increasing the applied voltage swaps from 0.6 V to 0.8 V and then to 1 V resulted in a significant drop of energy storage parameters and degradation of MSC performance (Figure 8).

The reason for degradation was revealed by a set of additional XRD reflections which appeared to be due to KI crystallization. Some changes in the relative intensity of two (001) -reflections of Mxene were also observed. The data suggest that iodine is intercalated into MXene interlayers and does not migrate significantly when the applied voltage is expected to drive it away from the structure.

Linear scan over the electrodes and the gap region demonstrated that the KI precipitation was significantly stronger over the working electrode and much less pronounced over the counter electrode. We note that adding some fresh electrolyte over the MSC device partially restored the electrochemical performance of the device. Therefore, the degradation of performance is likely connected to both sorption of iodine by MXene electrodes and degradation of the electrolyte due to crystallization of KI.

Summarizing the results obtained with KI + H<sub>2</sub>O gel electrolyte, combined XRF and XRD characterization demonstrated that the poor performance of MSC is explained by irreversible (under conditions of voltage swap) intercalation of iodine into the MXene structure and low stability of the electrolyte. Crystallization of KI from electrolyte preferentially over the

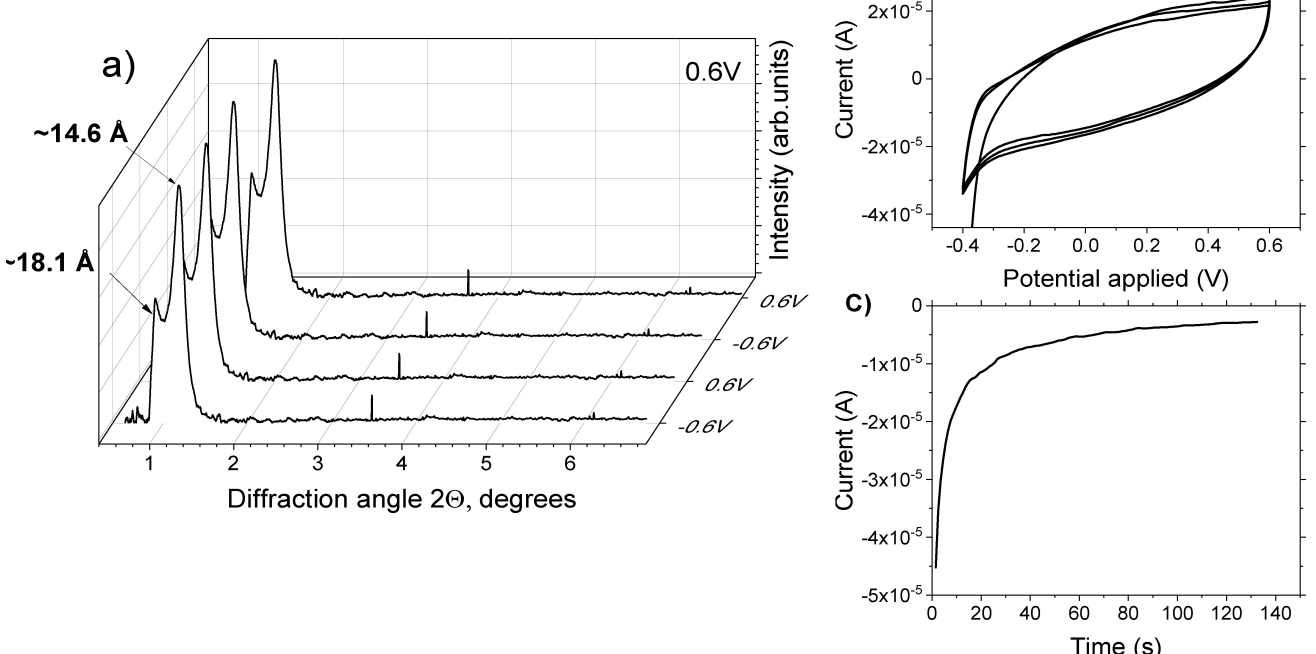


**Figure 7.** a) XRD patterns (background subtracted,  $\lambda=0.370 \text{ \AA}$ ) recorded from MXene CMSC in KI + H<sub>2</sub>O gel electrolyte under static conditions in fully charged state and swap of applied voltage from -0.6 V to +0.6 V, b) CV curves recorded from the cell prior to XRD tests (scan rate 30 mV/s) and example of charging curve recorded at given applied voltage prior to each XRD test.

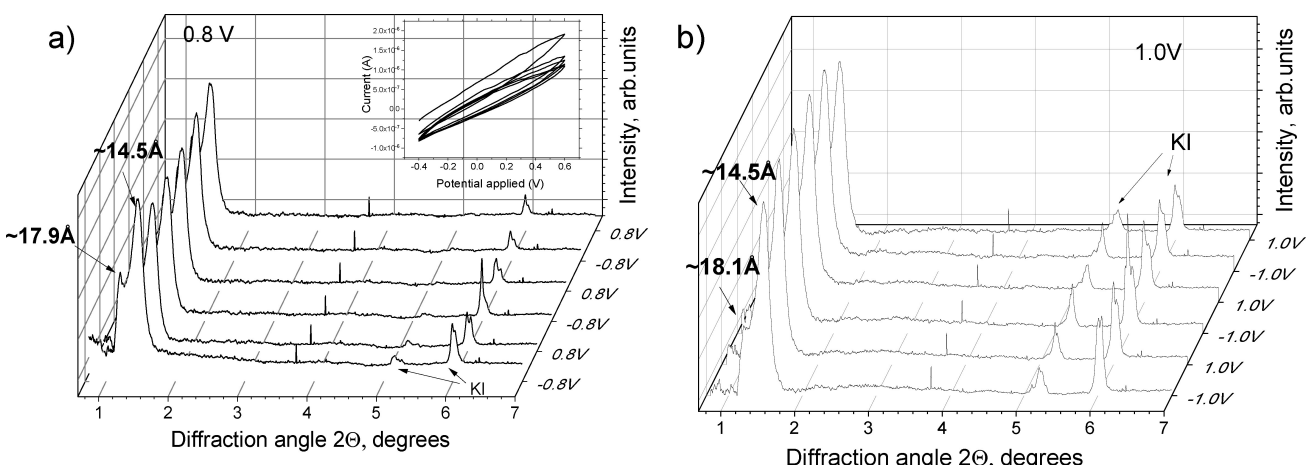


**Figure 8.** a) XRD patterns (background subtracted,  $\lambda=0.370\text{ \AA}$ ) recorded from working electrode of MXene CMSC in  $\text{KI}+\text{H}_2\text{O}$  gel electrolyte under static conditions in fully charged state and swap of applied voltage  $-0.8\text{ V}/+0.8\text{ V}$  (a) and  $-1.0\text{ V}/+1.0\text{ V}$ . Inset shows CV curve recorded with scan rate 30 mV/s

active electrode points out to voltage induced gel electrolyte degradation rather than simple evaporation of water as a reason for the observed loss of electrochemical performance.

#### In-Situ and In-Operando XRD Characterization of CMSC with KI + DMSO Electrolyte

Experiments with this type of electrolyte demonstrated the advantages of using synchrotron radiation XRD for *in-situ* and *in-operando* studies of MSC especially clearly. Figure 9 shows CV curves recorded from CMSC device directly after preparation in the standard for MXene supercapacitors voltage window  $-0.4\text{ V}$  to  $0.6\text{ V}$  and after set of experiments with XRD recorded from working electrode in fully charged state with swaps of applied voltage from positive to negative value (with counter electrode at  $0\text{ V}$ ). Considering the microscopic size of the device, it shows rather good performance directly after preparation when operated at standard voltage window  $0.6\text{ V}$ . The device was then subjected to voltage swaps between  $0.6\text{ V}$  and  $-0.6\text{ V}$  with XRD patterns recorded from working electrode in fully charged state (verified by control of charging current). The CV curves recorded after 3 full cycles with swap of applied voltage  $0.6\text{ V}/-0.6\text{ V}$  still showed the shape of curves close to rectangular (Figure 9b). Next experiments were performed with voltage intentionally increased over the values which are resulting in degradation of device performance.

The voltage was increased by  $0.1\text{ V}$  increments with swaps between positive and negative values at  $0.7\text{ V}$ ,  $0.8\text{ V}$ ,  $0.9\text{ V}$ ,  $1.0\text{ V}$ ,  $1.1\text{ V}$  and  $1.2\text{ V}$ . Linear scans and *in-operando* tests were also performed at some voltage values (see below). The CV curve recorded after testing with applied voltage up to  $1.2\text{ V}/-1.2\text{ V}$  is shown in (Figure 9c) and showed complete degradation of the device. However, the performance of the device could partly be restored by adding some fresh electrolyte over the device surface (Figure 9d).

The standard electrochemical characterization of CMSC shown in Figure 9 allows us to conclude that degradation of

device performance is mostly related to voltage increase but also partly due to ageing of electrolyte.

*In-situ* XRD characterization of MXene electrodes operated in KI-DMSO electrolyte allows us to detect structural changes that correlate with the decrease of the device performance. The CMSC device shows stable performance if operated at  $0.6\text{ V}/-0.6\text{ V}$  voltage window. The  $d(001)$  value of about  $18.6\text{ \AA}$  remained unchanged after voltage swaps in the studied spot located close to the gap at the working electrode (Figure 10). Linear scans recorded after  $0.6\text{ V}/-0.6\text{ V}$  voltage swaps also showed no shift in the position of  $(001)$  reflection, as shown in Figure 11. Some scatter in the  $d$ -values along the scan line is explained by the presence of diffraction spots in 2D images and somewhat asymmetric shape of integrated peaks.

In the next step we recorded XRD images directly in the process of recording CV curves (Figure 12). The XRD patterns were recorded continuously in this experiment throughout the full voltage cycle between  $0.6\text{ V}$  and  $-0.6\text{ V}$ . The  $d(001)$  value was found to be within the range of  $18.6\text{ \AA}-19.0\text{ \AA}$  during the whole cycle. No change in position of this reflection was detected after changing of voltage polarity. It can be concluded that the CMSC demonstrated stable performance under  $0.6\text{ V}/-0.6\text{ V}$  operation conditions.

Next experiments were performed with swaps at higher voltages. Starting from  $0.8\text{ V}$  some small but reproducible shifts in the  $(001)$  position were observed. About  $0.4\text{ \AA}$  smaller  $d(001)$  was recorded from the MXene electrode with positive applied potential compared to the negatively charged state. The difference between the XRD patterns recorded at a positive and negative potential is even stronger for data recorded at higher voltage. Figure 13 shows that  $(001)$ -reflections recorded at positive  $1\text{ V}$  potential are clearly asymmetric, lower in intensity and downshifted by  $\sim 1\text{ \AA}$  compared to patterns recorded at  $-1\text{ V}$ . Further increase of applied potential to  $1.1\text{ V}$  and  $1.2\text{ V}$  results in even lower intensity of all peaks and stronger difference between positions of  $(001)$  reflections recorded with positive and negative potential. The patterns recorded with negative potential also show additional shoulder with increased

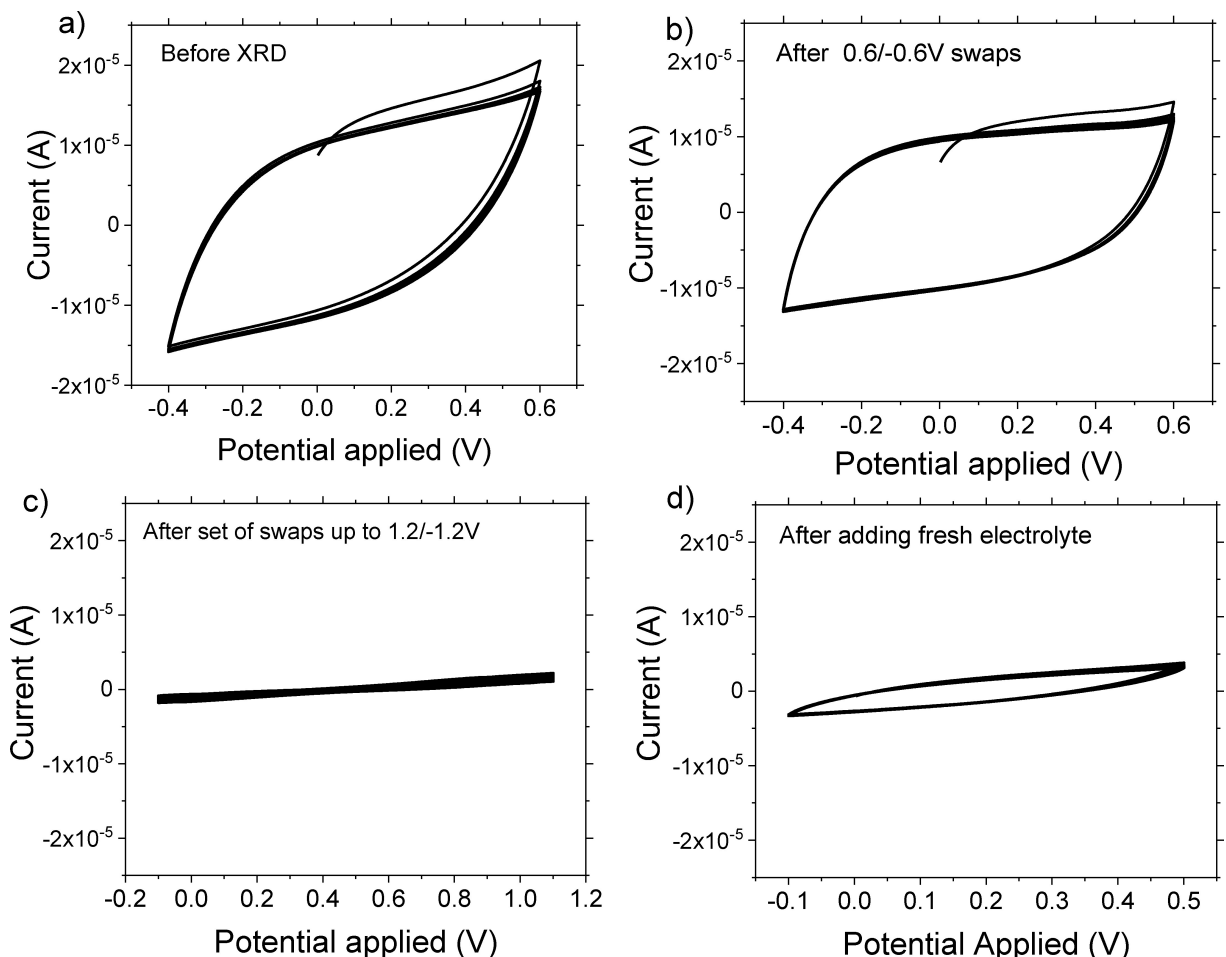


**Figure 9.** CV curves recorded at different moments of experiments with the same CMSC device with KI + DMSO gel electrolyte (scan rate 50 mV/s): a) directly after preparation of device; b) after recording XRD data from working MXene electrode with applied voltage swaps between 0.6 V and  $-0.6$  V in 3 cycles (see XRD data in the Figure 10 below); c) the same after voltage swaps at 0.7 V, 0.8 V, 0.9 V, 1.0 V, 1.1 V, 1.2 V (see Figure 10 below); d) the same sample after adding fresh electrolyte.

d(001) value of  $\sim 21.6$  Å. Nearly complete degradation of energy storage in the device was observed after swaps at 1.2V/ $-1.2$  V as evidenced by CV curves (Figure 9c) and by a decline of charging current to nearly negligible value after swap of potential.

The degradation of MXene electrodes due to excessively high applied voltage is a straightforward suggestion which appears to be only partly valid. Surprisingly, the structure of MXene electrodes and the performance of the device were partly restored after adding fresh gel electrolyte. (Figure 9d). The same device operated again at 1.2 V showed only one (001)-reflection at  $\sim 18.4$  Å (no shoulder at smaller angles) and almost no change after change of polarity to  $-1.2$  V (Figure 13).

Only one XRD reflection was observed for (001) on both sides of the gap, and in both scans the value of d-spacing was within 18.3 Å and 18.9 Å, similarly to the values observed from these electrodes prior to experiments with increased voltage (Figure 14). Energy storage of the device was also partly restored as evidenced by CV curves recorded at the standard potential window  $-0.4$  V to 0.6 V (Figure 9d).

It is interesting to discuss the possible reasons for the change in (001)-position and broadness due to the change of applied voltage polarity in KI-DMSO gel electrolyte observed in our experiments (Figure 10,13).

A small increase of MXene interlayer distance ( $\sim 0.3$  Å) due to electrochemical intercalation of potassium (in KOH electrolyte) was earlier reported for HF etched material.<sup>[10f]</sup> In our experiments both Li (intercalated into MXene after synthesis) and K cations are present in the system but no changes in the (001)-reflection due to electrochemical intercalation and deintercalation were observed.

The strong change in the structure of MXene electrode under conditions of potential swap can be explained considering that KI is a redox active electrolyte. The addition of KI to acidic electrolytes has been reported previously to result in an increase in energy storage of supercapacitors based on activated carbons<sup>[35]</sup> and, more recently, MXene.<sup>[36]</sup>

The redox electrolyte (KI) takes part in the redox reactions at the positive electrode, which was adopted to enhance the energy storage capacity of the positive electrodes and the MXene-based symmetric supercapacitors with the energy

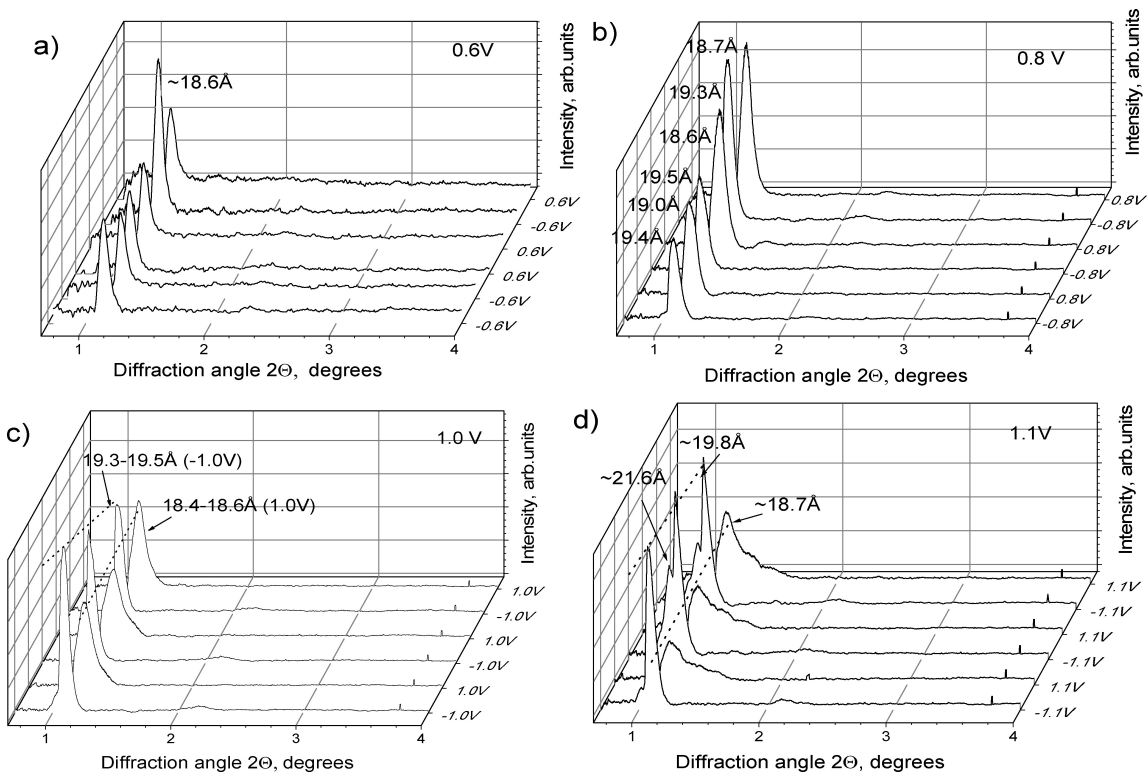


**Figure 10.** XRD patterns (background subtracted,  $\lambda = 0.370 \text{ \AA}$ ) recorded in situ from CMSC device ( $\text{KI} + \text{DMSO}$  gel electrolyte) from working electrode under static conditions of saturated charging with applied voltage swaps: (a)  $0.6 \text{ V} / -0.6 \text{ V}$ , (b)  $0.8 \text{ V} / -0.8 \text{ V}$ ; (c)  $1.0 \text{ V} / -1.0 \text{ V}$ , (d)  $1.1 \text{ V} / -1.1 \text{ V}$ . The data for voltage swaps  $0.7 / -0.7 \text{ V}$ ,  $0.9 \text{ V} / -0.9 \text{ V}$  and  $1.2 / -1.2 \text{ V}$  were also recorded in the same experiment (Figure S6).

storage mechanism changing from the capacitive type to the battery type.<sup>[26,37]</sup>

The redox active KI electrolyte is expected to provide electrochemical reactions that result in formation of  $\text{I}_2$  and  $\text{I}_3^-$ .<sup>[26,38]</sup>



However, CV loops recorded for MSC with  $\text{KI}-\text{H}_2\text{O}$  and  $\text{KI}-\text{DMSO}$  electrolytes do not reveal sharp features typical for KI redox reactions (Figures 7a, 9a, 12b). This effect can be explained if part of iodine was intercalated into MXene directly after addition of gel electrolyte. Iodine ions are likely to react with MXene surface groups while neutral  $\text{I}_2$  would not contribute to electrochemical performance. The CV loops are possibly related to migration of Li present in the sample due to synthesis procedure involving  $\text{LiCl}$ . Irreversible iodine intercalation is actually confirmed by XRF experiments (Figure 6).

It is interesting to note that earlier studies indicated absence of electrochemical intercalation of bromine and chlorine anions in experiments with MXene in a voltage range from  $-0.3$  to  $+0.5 \text{ V}$ .<sup>[39]</sup> This conclusion was supported among other methods by absence of changes in inter-layer distance of MXene in XRD experiments. Therefore, the changes of inter-layer distance observed in our experiments are likely to be specific for iodine reaction with MXene.

Inter-layer distance of about  $14-14.5 \text{ \AA}$  (in a solvent free state) was reported earlier for iodine intercalated Mxene  $\text{Ti}_3\text{C}_2\text{T}_x$ .<sup>[40]</sup> The MXene synthesized in this paper by iodine etching was found to exhibit an interlayer distance of  $14.4 \text{ \AA}$  after synthesis and  $17.4 \text{ \AA}$  after delamination in HCl. The lattice expansion (compared to pristine not functionalized MXene,  $\sim 12 \text{ \AA}$ ) by  $\sim 2.5 \text{ \AA}$  and by  $\sim 5.4 \text{ \AA}$  was assigned to functionalization of 2D MXene layers with iodine and formation of Ti-I bonds. However, exact structures of these phases (especially expanded one with inter-layer distance  $17.4 \text{ \AA}$ ) remain unclear. Considering that the length of Ti-F and Ti-I bonds are extremely similar, formation of  $\text{Ti}_3\text{C}_2\text{I}_x$  is not expected to result in an increase of inter-layer distance compared to standard MXene terminated by fluorine and oxygen-containing groups. Therefore, it is likely that MXene reported in this study was additionally expanded by iodine e.g., in a form  $\text{I}_2$  in the inter-layer space.<sup>[40]</sup>

Our in situ experiments with  $\text{KI}-\text{H}_2\text{O}$  gel electrolyte showed two phases with  $\sim 14.5 \text{ \AA}$  and  $17.9-18.1 \text{ \AA}$  directly after cycling in  $-0.4 \text{ V}$  to  $0.6 \text{ V}$  window. These phases were observed also after voltage swaps up to  $-1.0 \text{ V}/1.0 \text{ V}$ . Considering that  $14.5 \text{ \AA}$  is “pristine” water swollen state of MXene, increase by  $\sim 3 \text{ \AA}$  due to applied potential swaps is in agreement with irreversible iodine intercalation suggested by XRD and XRF data.

More complex phase composition was found for MXene in  $\text{KI}-\text{DMSO}$  electrolyte where some reversible cycling effect was observed for potential swaps above  $+0.8 \text{ V}/-0.8 \text{ V}$ .

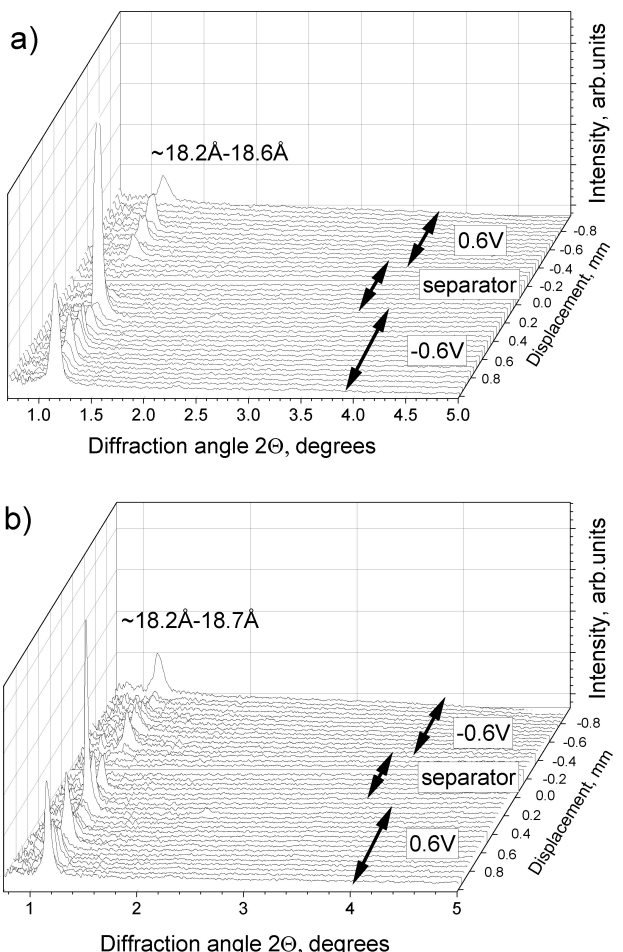


**Figure 11.** XRD patterns (background subtracted,  $\lambda = 0.370 \text{ \AA}$ ) recorded in the linear scan over the working electrode (charged at 0.6 V (a) and -0.6 V (b)), material free gap and counter electrode (0 V). The patterns were recorded over 2 mm with 0.1 mm steps in a direction perpendicular to gap zone. XRD pattern recorded in the middle of material-free gap was used to subtract background. (KI + DMSO gel electrolyte).

Interlayer distance of  $\sim 18.0\text{--}18.5 \text{ \AA}$  is typical for DMSO swollen MXene (Figure S2).<sup>[10b]</sup> Observation of additional reflections with d-spacings  $19.5 \text{ \AA}$  and  $21.6 \text{ \AA}$  in KI-DMSO gel electrolyte are likely to originate from iodine intercalation. Our experiments demonstrate additional expansion of MXene structure at positive applied potential ( $> 0.8 \text{ V}$ ). When a negative potential is applied, the d(001) value changes to almost the same as in pristine MXene state but the (001) reflection is broad and weak.

Most likely two separate processes are observed in our experiments with KI-DMSO electrolyte: first is irreversible functionalization of MXene surface with iodine (with formation of  $\text{Ti}_3\text{C}_2\text{-I}_x$ ) and second is reversible intercalation of iodine under conditions of voltage swaps ( $> 0.8 \text{ V}$ ) forming iodine-intercalated structure. Substitution of surface functional groups of MXene is not likely to lead to expansion of inter-layer distance since e.g. Ti–F and Ti–I bond length is essentially the same. Therefore, expanded MXene structures must be related to some other mechanism of iodine intercalation, e.g. as  $\text{I}_3^-$ .

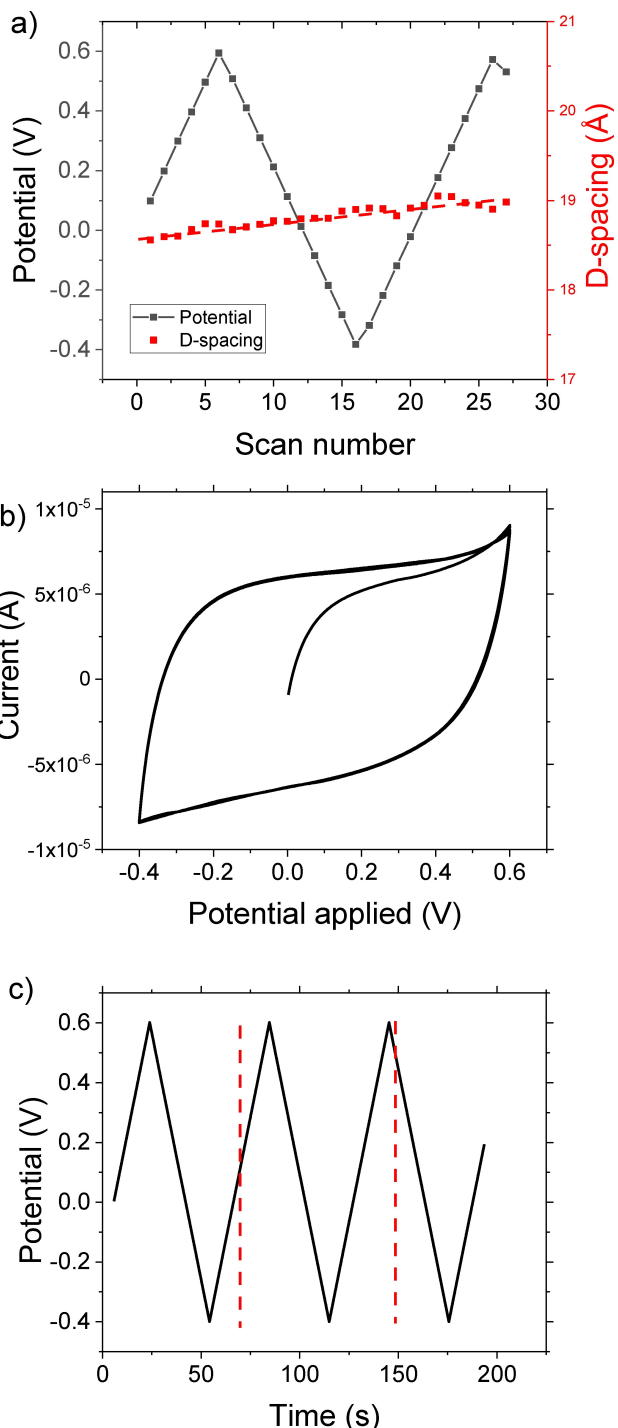


**Figure 12.** a) In-operando XRD characterization of MXene electrode in SMCS with KI-DMSO gel electrolyte recorded in 0.6 V to 0–0.6 V voltage window. a) Voltage change profile and d(001) values recorded during the full cycle. b) CV curve recorded with scan rate 33 mV/s and c) time profile of the whole experiment with dashed line showing interval where XRD patterns were recorded from working electrode.

Appearance of additional MXene structures also correlates with nearly complete degradation of energy storage of MSC device (Figure 9C).

It should be noted that relatively thin layer of gel electrolyte was added over the electrodes due to cylindrical shape

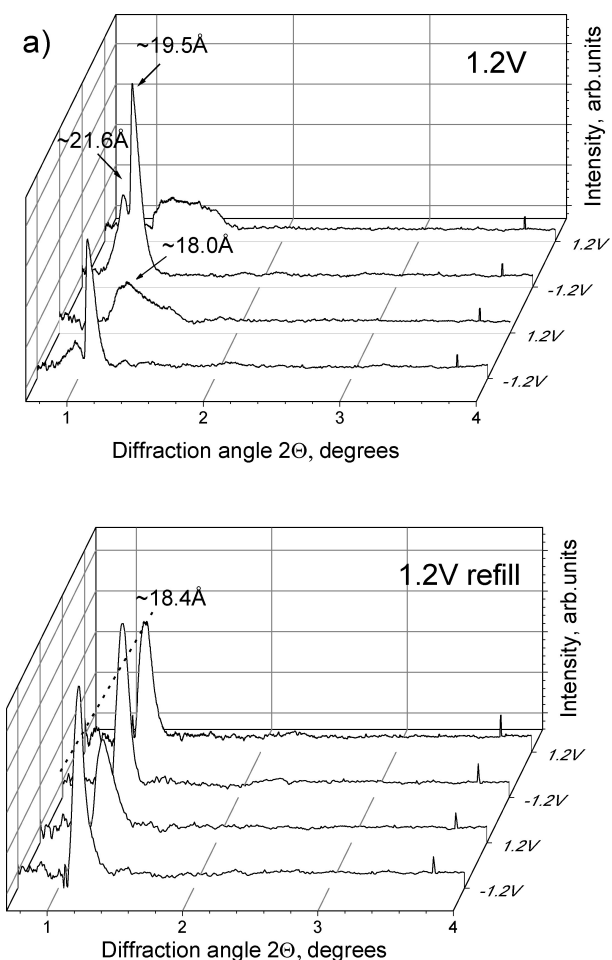


**Figure 13.** XRD patterns (background subtracted,  $\lambda = 0.370 \text{ \AA}$ ) recorded from working electrode in fully charged state under applied voltages 1.2 V / -1.2 V a) before and b) after adding fresh electrolyte.

enhancing possible effects related to the depletion of electrolyte due to MXene functionalization with iodine.

Therefore, we suggest that electrochemical cycling in combination with gel ageing results in depletion of electrolyte from mobile ions due to sorption of iodine (and potassium as counter ions) by MXene electrodes. Irreversible sorption of iodine by MXene electrodes was confirmed also in XRF experiments.

This interpretation of data suggests that independently on the polarity of applied potential, large part of iodine remains intercalated in MXene lattice. Therefore, (001) reflections corresponding to expanded inter-layer distance (up to 21.6 Å) are related to voltage induced intercalation of  $I_3^-$  anions. Note that the expansion of MXene lattice becomes gradually stronger after experiments with increase applied voltage reflecting larger and larger part of iodine moving from electrolyte into chemically bound state. Adding fresh electrolyte suggestively allows to dissolve some iodine intercalated in MXene interlayers and to restore pristine DMSO-swollen state of MXene with inter-layer distance of about 18.5 Å.

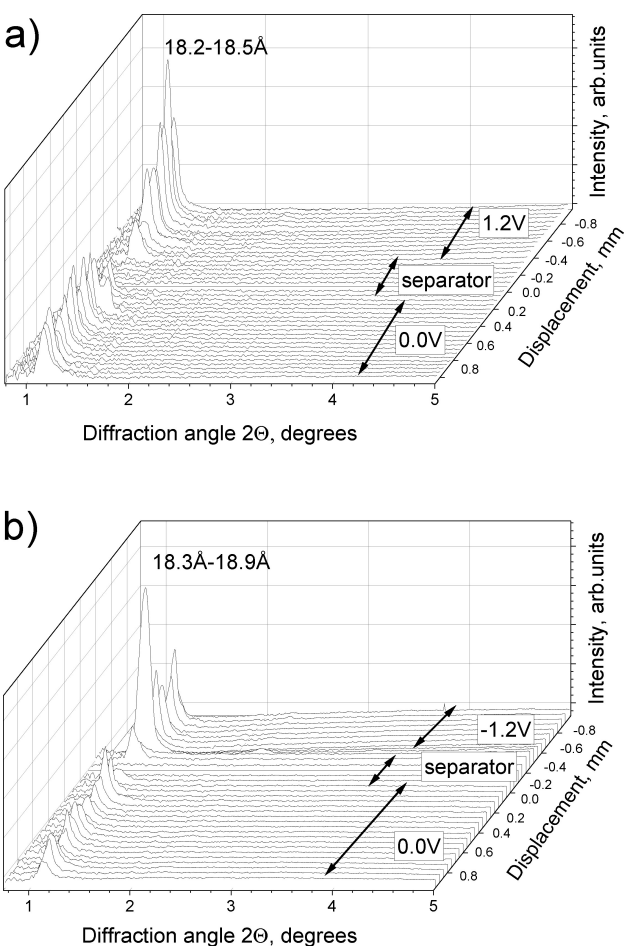


**Figure 14.** XRD patterns (background subtracted,  $\lambda = 0.370 \text{ \AA}$ ) recorded in linear scan over the working electrode (charged at 1.2 V (a) and -1.2 V (b)), gap and counter electrode (0 V). The patterns were recorded along 2 mm path with 0.1 mm steps in a direction perpendicular to gap zone. XRD patterns recorded in the material-free gap was used to subtract background.

Additional experiments are required to verify exact mechanism of MXene structure breathing under the change of voltage polarity in KI based electrolytes.

## Conclusions

In summary, synchrotron radiation XRD with nano-sized beam was used for *in-situ* and *in-operando* characterization of MXene electrodes in MSC devices with design optimized for recording data in transmission mode. A microscopic electrochemical cell was painted directly over the surface of standard glass capillaries and used for recording synchrotron radiation XRD data for MSC with four types of PVA-based gel electrolytes. The standard for MXene MSC  $H_2SO_4-H_2O/PVA$  electrolyte was demonstrated also as best for structural stability of MXene electrodes. No changes of inter-layer distance were detected for MXene electrodes in this electrolyte with applied voltages up to 1 V, no changes detected if the polarity of applied voltage was swapped between negative and positive values in several

cycles, no changes of structure were also detected under conditions of MSC operation during charging and discharging.

In contrast, replacing water with DMSO as solvent for  $\text{H}_2\text{SO}_4$  results in degradation of MXene electrodes at applied voltages 0.9 V/–0.9 V. Voltage-induced swelling of MXene with irreversible insertion of additional layer of DMSO was detected by *in situ* XRD and suggested as a structural reason for collapse of MSC performance.

A two-phase MXene electrode structure was also detected in KI- $\text{H}_2\text{O}$  electrolyte, independently on polarity of applied voltage already at 0.6 V/–0.6 V. Two (001)-reflections with  $\sim 3$ –3.5 Å difference indicate inhomogeneous intercalation of ions in hydrated state. Increasing the applied voltage to 0.8 V resulted in degradation of electrochemical performance due to partial crystallization of KI in the gel electrolyte.

Extended *in-situ* and *in-operando* experiments were performed also for MXene CMSC with KI-DMSO electrolyte. No changes in MXene structure and stable performance of MSC were observed at 0.6 V/–0.6 V. Charging and discharging cycles performed at higher voltages revealed voltage induced expansion of MXene structure at negatively charged electrode with formation of two-phase mixture. The changes between values of d(001) recorded on positively charged electrode and on negatively charged electrode ( $\sim 2$  Å and 3.6 Å) are likely related to intercalation and de-intercalation of iodine formed in redox active KI-DMSO gel electrolyte. The pristine MXene phase with d(001)=16.4 Å was restored after addition of fresh gel electrolyte in correlation with partial recover of CV loops and energy storage performance.

Our experiments prove that *in-situ* and *in-operando* XRD can also be used to study the structure of MXene electrodes using linear scans performed with 0.1 mm displacement steps along a path crossing both electrodes and charge separation zone. It can be concluded that *in-situ* and *in-operando* XRD can be used to detect structural modification of MXene electrodes in MSC under conditions of applied charge and under operating conditions. The cylindrical design of MSC devices developed in our experiments is advised for experiments with transmission mode XRD. This design can very likely be useful also for studies of other types of electrochemical devices.

Finally, we also demonstrated the feasibility of 2D element mapping in MSC devices using XRF applied to standard in-plane MSC with KI-based gel electrolyte. Strong sorption of iodine by MXene was detected when a rather thin electrolyte layer was added over electrodes, thus depleting the gel from iodine. Some changes in iodine concentration could also be detected using much thicker electrolyte droplet. However, a precise control of gel electrolyte thickness is required in order to obtain more information using XRF.

## Supporting Information

Supporting information for this article is given via a link at the end of the document. It includes additional characterization of precursor MXene, schemes of experimental setups, additional data for synchrotron radiation XRD experiments with MSC.

## Acknowledgements

A.T. acknowledges funding from the European Union's Horizon 2020 Research and Innovation Program (Grant No. 881603) and Energimyndigheten (Grant No. 50620-1). The authors also acknowledge the Vibrational Spectroscopy Platform of Umeå University and A. Shchukarev for support with the XPS measurements. We acknowledge the ESRF for providing synchrotron radiation beam time (experiment number: MA5528) on ID16b.

## Conflict of Interests

The authors declare no conflict of interest.

## Data Availability Statement

The data that support the findings of this study are available from the corresponding author upon reasonable request.

**Keywords:** MXene · supercapacitor · *in situ* · *in operando* · XRD

- [1] a) J. Nelson, S. Misra, Y. Yang, A. Jackson, Y. J. Liu, H. L. Wang, H. J. Dai, J. C. Andrews, Y. Cui, M. F. Toney, *J. Am. Chem. Soc.* **2012**, *134*, 6337–6343; b) D. Q. Liu, Z. Shadike, R. Q. Lin, K. Qian, H. Li, K. K. Li, S. W. Wang, Q. P. Yu, M. Liu, S. Ganapathy, X. Y. Qin, Q. H. Yang, M. Wagemaker, F. Y. Kang, X. Q. Yang, B. H. Li, *Adv. Mater.* **2019**, *31*, 1806620.
- [2] B. Pal, A. Yasin, R. Kaur, M. Tebyetekerwa, F. Zabihi, S. Y. Yang, C. C. Yang, Z. Sofer, R. Jose, *Renew Sust Energ Rev* **2021**, *149*, 111418.
- [3] G. P. Wang, L. Zhang, J. J. Zhang, *Chem. Soc. Rev.* **2012**, *41*, 797–828.
- [4] A. Gonzalez, E. Goikolea, J. A. Barrena, R. Mysyk, *Renew Sust Energ Rev* **2016**, *58*, 1189–1206.
- [5] a) E. Frackowiak, Q. Abbas, F. Béguin, *J. Energy Chem.* **2013**, *22*, 226–240; b) Z. Heidarinejad, M. H. Dehghani, M. Heidari, G. Javedan, I. Ali, M. Sillanpää, *Environ. Chem. Lett.* **2020**, *18*, 393–415.
- [6] a) F. W. Richey, B. Dyatkin, Y. Gogotsi, Y. A. Elabd, *J. Am. Chem. Soc.* **2013**, *135*, 12818–12826; b) G. Oukali, E. Salager, M. R. Ammar, C. E. Dutoit, V. Sarou-Kanian, P. Simon, E. Raymundo-Piñero, M. Deschamps, *ACS Nano* **2019**, *13*, 12810–12815; c) H. Wang, A. C. Forse, J. M. Griffin, N. M. Trease, L. Trognko, P. L. Taberna, P. Simon, C. P. Grey, *J. Am. Chem. Soc.* **2013**, *135*, 18968–18980; d) A. C. Forse, J. M. Griffin, C. Merlet, J. Carretero-Gonzales, A.-R. O. Raji, T. N. M. C. P. Grey, *Nat. Energy* **2017**, *2*, 1–7; e) M. Salanne, B. Rotenberg, K. Naoi, K. Kaneko, P. L. Taberna, C. P. Grey, B. Dunn, P. Simon, *Nat. Energy* **2016**, *1*, 16070.
- [7] A. Johannes, D. Salomon, G. Martinez-Criado, M. Glaser, A. Lugstein, C. Ronning, *Sci. Adv.* **2017**, *3*.
- [8] Z. F. Lin, P. Rozier, B. Dupoyer, P. L. Taberna, B. Anasori, Y. Gogotsi, P. Simon, *Electrochem. Commun.* **2016**, *72*, 50–53.
- [9] X. Wang, T. S. Mathis, K. Li, Z. Lin, L. Vlcek, T. Torita, N. C. Osti, C. Hatter, P. Urbankowski, A. Sarycheva, M. Tyagi, E. Mamontov, P. Simon, Y. Gogotsi, *Nat. Energy* **2019**, *4*, 241–248.
- [10] a) L. Verger, V. Natu, M. Ghidiu, M. W. Barsoum, *J. Phys. Chem. C* **2019**, *123*, 20044–20050; b) A. Iakunkov, A. Nordenstrom, N. Boulanger, C. Hennig, I. Baburin, A. V. Talyzin, *Nanoscale* **2022**, *14*, 10940–10949; c) C. A. Voigt, M. Ghidiu, V. Natu, M. W. Barsoum, *J. Phys. Chem. C* **2018**, *122*, 23172–23179; d) S. Celrier, S. Hurand, C. Garnero, S. Morisset, M. Benchakar, A. Habrioux, P. Chartier, V. Mauchamp, N. Findling, B. Lanson, E. Ferrage, *Chem. Mater.* **2019**, *31*, 454–461; e) S. Doo, A. Chae, D. Kim, T. Oh, T. Y. Ko, S. J. Kim, D. Y. Koh, C. M. Koo, *Acs Appl Mater Inter* **2021**, *13*, 22855–22865; f) M. R. Lukatskaya, O. Mashtalir, C. E. Ren, Y. Dall'Agnese, P. Rozier, P. L. Taberna, M. Naguib, P. Simon, M. W. Barsoum, Y. Gogotsi, *Science* **2013**, *341*, 1502–1505.
- [11] a) C. Zhan, M. Naguib, M. Lukatskaya, P. R. C. Kent, Y. Gogotsi, D. E. Jiang, *J. Phys. Chem. Lett.* **2018**, *9*, 1223–1228; b) M. R. Lukatskaya, S. M. Bak, X. Q. Yu, X. Q. Yang, M. W. Barsoum, Y. Gogotsi, *Adv. Energy Mater.* **2015**, *5*, 15000589.

- [12] a) A. V. Mohammadi, J. Rosen, Y. Gogotsi, *Science* **2021**, *372*, 1165; b) Z. X. Li, C. Ma, Y. Y. Wen, Z. T. Wei, X. F. Xing, J. M. Chu, C. C. Yu, K. L. Wang, Z. K. Wang, *Nano Res.* **2020**, *13*, 196–202; c) Y. Gogotsi, B. Anasori, *ACS Nano* **2019**, *13*, 8491–8494.
- [13] a) Q. Jiang, Y. Lei, H. Liang, K. Xi, C. Xia, H. N. Alshareef, *Energy Storage Mater.* **2020**, *27*, 78–95; b) B. Yang, L. Wang, M. Zhang, J. Luo, Z. Lu, X. Ding, *Adv. Funct. Mater.* **2020**, *30*, 2000186.
- [14] M. Ghidiu, M. R. Lukatskaya, M. Q. Zhao, Y. Gogotsi, M. W. Barsoum, *Nature* **2014**, *516*, 78–81.
- [15] a) Y. Xie, H. Zhang, H. Huang, Z. Wang, Z. Xu, H. Zhao, Y. Wang, N. Chen, W. Yang, *Nano Energy* **2020**, *74*, 104928; b) Q. Jiang, Y. J. Lei, H. F. Liang, K. Xi, C. Xia, H. N. Alshareef, *Energy Storage Mater.* **2020**, *27*, 78–95; c) M. L. Wang, S. X. Feng, C. Bai, K. Ji, J. X. Zhang, S. L. Wang, Y. Q. Lu, D. S. Kong, *Small* **2023**, *19*, 2300386; d) P. Salles, E. Quain, N. Kurra, A. Sarycheva, Y. Gogotsi, *Small* **2018**, *14*, 1802864.
- [16] C. X. Meng, P. Das, X. Y. Shi, Q. Fu, K. Mullen, Z. S. Wu, *Small Sci* **2021**, *1*, 2000076.
- [17] a) N. Jackel, B. Kruner, K. L. Van Aken, M. Alhabeb, B. Anasori, F. Kaasik, Y. Gogotsi, V. Presser, *ACS Appl. Mater. Interfaces* **2016**, *8*, 32089–32093; b) Z. Lin, P. Rozier, B. Dupoyer, P.-L. Taberna, B. Anasori, Y. Gogotsi, P. Simon, *Electrochem. Commun.* **2016**, *72*, 50–53.
- [18] a) H. Shao, K. Xu, Y. C. Wu, A. Iadecola, L. Y. Liu, H. Y. Ma, L. T. Qu, E. Raymundo-Pinero, J. X. Zhu, Z. F. Lin, P. L. Taberna, P. Simon, *ACS Energy Lett.* **2020**, *5*, 2873–2880; b) M. D. Levi, M. R. Lukatskaya, S. Sigalov, M. Beidaghi, N. Shpigel, L. Daikhin, D. Aurbach, M. W. Barsoum, Y. Gogotsi, *Adv. Energy Mater.* **2015**, *5*, 1400815; c) T. B. Sobyra, K. Matthews, T. S. Mathis, Y. Gogotsi, P. Fenter, *ACS Energy Lett.* **2022**, *7*, 3612–3617; d) Y. Zhu, S. Zheng, P. Lu, J. Ma, P. Das, F. Su, H. M. Cheng, Z. S. Wu, *Natl. Sci. Rev.* **2022**, *9*, nwac024; e) X. P. Mu, D. S. Wang, F. Du, G. Chen, C. Z. Wang, Y. J. Wei, Y. Gogotsi, Y. Gao, Y. Dall'Agnese, *Adv. Funct. Mater.* **2019**, *29*; f) Y. Dall'Agnese, P. Rozier, P. L. Taberna, Y. Gogotsi, P. Simon, *J. Power Sources* **2016**, *306*, 510–515.
- [19] a) N. A. Kyeremateng, T. Brousse, D. Pech, *Nat. Nanotechnol.* **2017**, *12*, 7–15; b) D. P. Qi, Y. Liu, Z. Y. Liu, L. Zhang, X. D. Chen, *Adv. Mater.* **2017**, *29*, 1702800.
- [20] C. F. J. Zhang, S. Pinilla, N. McEyoy, C. P. Cullen, B. Anasori, E. Long, S. H. Park, A. Seral-Ascaso, A. Shmeliov, D. Krishnan, C. Morant, X. H. Liu, G. S. Duesberg, Y. Gogotsi, V. Nicolosi, *Chem. Mater.* **2017**, *29*, 4848–4856.
- [21] R. A. Soomro, P. Zhang, B. M. Fan, Y. Wei, B. Xu, *Nano-Micro Lett.* **2023**, *15*, 108.
- [22] a) M. Micusik, M. Slouf, A. Stepura, Y. Soyka, E. Ovodok, M. Procházka, M. Omastová, *Appl. Surf. Sci.* **2023**, *610*, 155351; b) S. Seyedin, J. Z. Zhang, K. A. S. Usman, S. Qin, A. M. Glushenkov, E. R. S. Yanza, R. T. Jones, J. M. Razal, *Glob. Chall.* **2019**, *3*, 1900037.
- [23] T. Habib, X. F. Zhao, S. A. Shah, Y. X. Chen, W. M. Sun, H. An, J. L. Lutkenhaus, M. Radovic, M. J. Green, *NPJ 2D Mater. Appl.* **2019**, *3*, 8.
- [24] a) Z. S. Wu, K. Parvez, X. L. Feng, K. Müllen, *Nat. Commun.* **2013**, *4*; b) J. T. Li, S. S. Delektta, P. P. Zhang, S. Yang, M. R. Lohe, X. D. Zhuang, X. L. Feng, M. Östling, *ACS Nano* **2017**, *11*, 8249–8256; c) Y. T. Xie, H. T. Zhang, H. C. Huang, Z. X. Wang, Z. Xu, H. B. Zhao, Y. C. Wang, N. J. Chen, W. Q. Yang, *Nano Energy* **2020**, *74*, 104928.
- [25] M. R. Lukatskaya, S. Kota, Z. F. Lin, M. Q. Zhao, N. Shpigel, M. D. Levi, J. Halim, P. L. Taberna, M. Barsoum, P. Simon, Y. Gogotsi, *Nat. Energy* **2017**, *2*, 17105.
- [26] Y. P. Tian, C. H. Yang, Y. Y. Luo, H. Y. Zhao, Y. P. Du, L. B. Kong, W. X. Que, *ACS Appl. Energ. Mater.* **2020**, *3*, 5006–5014.
- [27] Y. Marcus, *Chem. Rev.* **1988**, *88*, 1475–1498.
- [28] A. Iakunkov, U. Lienert, J. H. Sun, A. V. Talyzin, *Adv. Sci.* **2024**, *11*, 2307067.
- [29] a) K. Devineau, I. Bihannic, L. Michot, F. Villiéras, F. Masrouri, O. Cuisinier, G. Fragneto, N. Michau, *Appl. Clay Sci.* **2006**, *31*, 76–84; b) T. J. Tambach, P. G. Bolhuis, B. Smit, *Angew. Chem. Int. Ed.* **2004**, *43*, 2650–2652.
- [30] A. V. Talyzin, S. M. Luzan, T. Szabó, D. Chernyshev, V. Dmitriev, *Carbon* **2011**, *49*, 1894–1899.
- [31] J. Tang, T. S. Mathis, N. Kurra, A. Sarycheva, X. Xiao, M. N. Hedhili, Q. Jiang, H. N. Alshareef, B. M. Xu, F. Pan, Y. Gogotsi, *Angew. Chem. Int. Ed.* **2019**, *58*, 17849–17855.
- [32] O. Mashtalir, M. Naguib, V. N. Mochalin, Y. Dall'Agnese, M. Heon, M. W. Barsoum, Y. Gogotsi, *Nat. Commun.* **2013**, *4*, 1716.
- [33] C. Körnig, T. Stauffer, O. Schmutzler, T. Bedke, A. Machicote, B. B. Liu, Y. Liu, E. Gargioni, N. Feliu, W. J. Parak, S. Huber, F. Grüner, *Sci. Rep.* **2022**, *12*, 2903.
- [34] D. D. Wang, W. H. Guo, J. M. Hu, F. Liu, L. S. Chen, S. W. Du, Z. K. Tang, *Sci. Rep.* **2013**, *3*, 1486.
- [35] a) S. T. Senthilkumar, R. K. Selvan, Y. S. Lee, J. S. Melo, *J. Mater. Chem. A* **2013**, *1*, 1086–1095; b) M. Eredia, S. Bellani, M. I. Zappia, L. Gabatell, V. Galli, A. Bagheri, H. Beydaghi, G. Bianca, I. Conticello, V. Pellegrini, F. Bonaccorso, *APL Mater.* **2022**, *10*, 101102; c) X. F. Wang, R. S. Chandrabose, S. E. Chun, T. Q. Zhang, B. Evanko, Z. L. Jian, S. W. Boettcher, G. D. Stucky, X. L. Ji, *Acs Appl Mater Inter* **2015**, *7*, 19978–19985.
- [36] a) J. Fu, L. Li, D. Lee, J. M. Yun, B. K. Ryu, K. H. Kim, *Appl. Surf. Sci.* **2020**, *504*, 144250; b) J. Wang, L. L. Hao, J. W. Qin, X. Zhang, Y. Cheng, L. F. Yue, Y. X. Wang, M. X. Jiang, Z. H. Wang, M. H. Cao, *Energy Storage Mater.* **2024**, *66*, 103209.
- [37] K. V. Sankar, R. K. Selvan, *Carbon* **2015**, *90*, 260–273.
- [38] A. I. Popov, D. H. Geske, *J. Am. Chem. Soc.* **1958**, *80*, 5346–5349.
- [39] N. Shpigel, A. Chakraborty, F. Malchik, G. Bergman, A. Nimkar, B. Gavriel, M. Turgeman, C. N. Hong, M. R. Lukatskaya, M. D. Levi, Y. Gogotsi, D. T. Major, D. Aurbach, *J. Am. Chem. Soc.* **2021**, *143*, 12552–12559.
- [40] H. H. Shi, P. P. Zhang, Z. C. Liu, S. Park, M. R. Lohe, Y. P. Wu, A. S. Nia, S. Yang, X. L. Feng, *Angew. Chem. Int. Ed.* **2021**, *60*, 8689–8693.

Manuscript received: February 8, 2024

Accepted manuscript online: May 20, 2024

Version of record online: July 16, 2024